Abstract

Manufacturing Automation Laboratories Inc. provides the metal cutting industry with advanced physics-based software to simulate and optimize cutting conditions used for machining. The science-based digital machining technology aims to maximize the material removal rate without chatter and damage to the machine tool, part, and tool. The work material properties, tool geometry, machine tool's torque – power, and stiffness are considered in estimating the most suitable cutting conditions for the NC part programming process. Technology is science-based and its theoretical principles are difficult to be understood by practicing process planners and machining personnel in industry. This project will be used to illustrate the fundamental principles of digital machining technology in layman's terms with step-by-step applications in industry.

In this project, a sample thin-walled part made from Aluminium is selected. Based on the part geometry, four end mills are selected. Impact testing of all four tools was conducted to measure their Frequency Responses on a DMU 50 5 axis CNC Machining center with an HSKA63 interface. The stiffness, damping, and natural frequencies are identified using a manual method as well as with CUTPRO commercial software of MAL Inc. The chatter vibration stability diagrams are also calculated manually as well as with CUTPRO. Chatter-free depth of cuts and spindle speeds are identified and experimentally validated before using them in the NC Part programming stage in NX's CAM system. The generated NC tool path is further optimized using NX's integrated NPRO digital machining software of MAL Inc. The NC part program without Npro optimization took 33 minutes and 21 seconds while the optimized part was machine in 32 minutes and 40 seconds with 2% productivity improvement without any chatter and overload of the tool.

ACKNOWLEDGEMENT

I am grateful to MAL Inc. for providing the project and knowledge required for the digital machining project. I was assisted by Nima Dabiri (BASc, MASc) for providing impact and cutting tests conducted on the DMU 50 CNC machining center at the Manufacturing Automation Laboratory in UBC. Dr. Yusuf Altintas taught the cutting mechanics, modal analysis and chatter stability basics which were used in this project. He also helped me in organizing the project and editing.

Steven McMillan kindly helped me with the scope and supervision of the project.

Chapter 1- Introduction

At present, NC part programs are prepared based on past machining experience and practice in the industry. Planners select cutting speeds, feeds, depth, and width of cuts based on past experience and recommendations found in tool catalogues. Tools are selected, the NC part program is prepared and tried on the machine. If the results are unsatisfactory, the NC part program is modified and tried again until a satisfactory result is achieved. Such a trial-and-error approach is not only time-consuming, it may lead to high scrap rates and low productivity in industry. It is especially not feasible in the aerospace industry where the machining cycle times are high and the parts are too costly to scrap in trials. As a result, the planners select highly conservative metal removal conditions which hinder productivity.

Digital machining aims to identify the most optimal cutting conditions using science-based principles ahead of costly physical trials. Even test trials need to be carried out in a cost-free virtual environment and the final NC part program must be generated correctly and most productively before physical machining. The Manufacturing Automation Laboratory at the University of British Columbia developed such a technology, which is packaged as industrial software tools by its spin-off company MAL Inc (www.malinc.com) and marketed worldwide. The technology is applied in industry in two steps as follows, where a typical thin-walled part is shown in Figure 1.

Step 1) The structural dynamics of the machine with the holder and tool are identified with impact hammer tests. The measurements are used to identify the natural frequencies, damping ratios, and stiffnesses at the tooltip where cutting takes place. Chatter-free depth – width of cuts and spindle speeds are estimated using the dynamic measurement of the machine, work material properties, and tool geometry. The predicted parameters are tested in short-cutting trials to ensure that the model is correct. The most feasible and chatter-free cutting conditions are used by the planner to generate NC Part programs in CAM systems. This step requires the use of CUTPRO Advanced Machining Simulation software developed by MAL Inc.

Step 2) Since the part geometry changes along the tool path, it is important to virtually test the performance of the NC part program in the CAM environment. The cutting forces, torque, power, bearing loads, chip loads per tooth, tool deflections, and possible chatter locations along the tool path are simulated as a virtual machining experiment. The CAM programmer can see the problematic zones along the tool path, and correct the machining strategy. Also, the process planners can set the maximum force, torque, power, and chip load and schedule the feed automatically along the tool path.

The optimized NC part program is then used in production to achieve minimum machining cycle time and maximum productivity without damaging the tool, part, and machine. The principles behind the engineering steps are explained in layman's terms in the following sections.

Chapter 2 - Digital machining-based process planning

The thin-walled aerospace part shown in Figure 1 is machined on a five-axis DMU 50 CNC Machining center controlled by a Siemens 840D CNC shown in Figure 2. Ideally, the lowest cycle time with the least amount of tools is desired to be used. Four balanced tools will be used to machine the part as listed in Table 1. The pictures of end mills mounted on the machine with various mechanical tool holders are shown in Figure 2. An impact blow is applied to the tool, and the resulting measured impact force and vibrations are shown in Figure 8. The process of generating chatter stability diagrams that show chatter-free depth of cut, width of cut, and spindle speeds is shown in Figure 11. Any depth of cut and speed above the diagram will result in chatter, and the cutting conditions below the diagram will lead to stable, chatter free good cuts. The chatter-free cutting conditions will be selected that will lead to the maximum material removal rate.

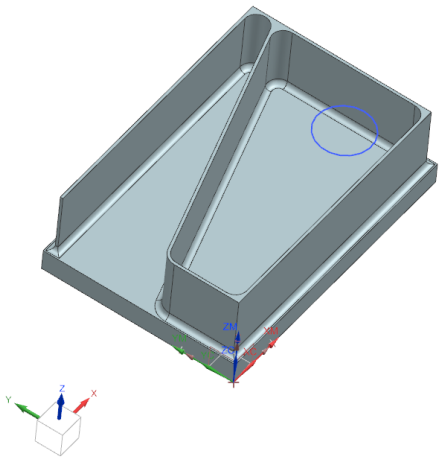

Figure 1 A thin walled part to be machined from Aluminum Al7050-T7451 material.

Table 1 Cutting tools used in machining the part.

Tool #	D [mm]	Teeth	Corner Radius [mm]	Stick-out Length [mm]	Helix Angle [deg]	Radial Rake Angle [deg]	Flute Height [mm]	Serration Pitch	Serration Amplitude
1	20	4	0.0	55.6	40	10.5	38	1.50	0.65
2	15.875	5	2.3	47.1	28	8	42	N/A	N/A
3	10	2	0.0	44.9	25	13.5	18	N/A	N/A
4	10	5	3.0	43.3	30	5	23.1	N/A	N/A

Figure 2 DMG Mori DMU 50 5 Axis CNC Machining center located at UBC. Cutting tools mounted on the spindle with mechanical chucks, hardware

2.1- Milling Process Mechanics

Milling tools have *N* number of teeth and they rotate at spindle speed *n(rev/min)* and linearly move at the programmed feed speed of *f(*mm/min) as shown in Figure 3. The feed per tooth is evaluated as:

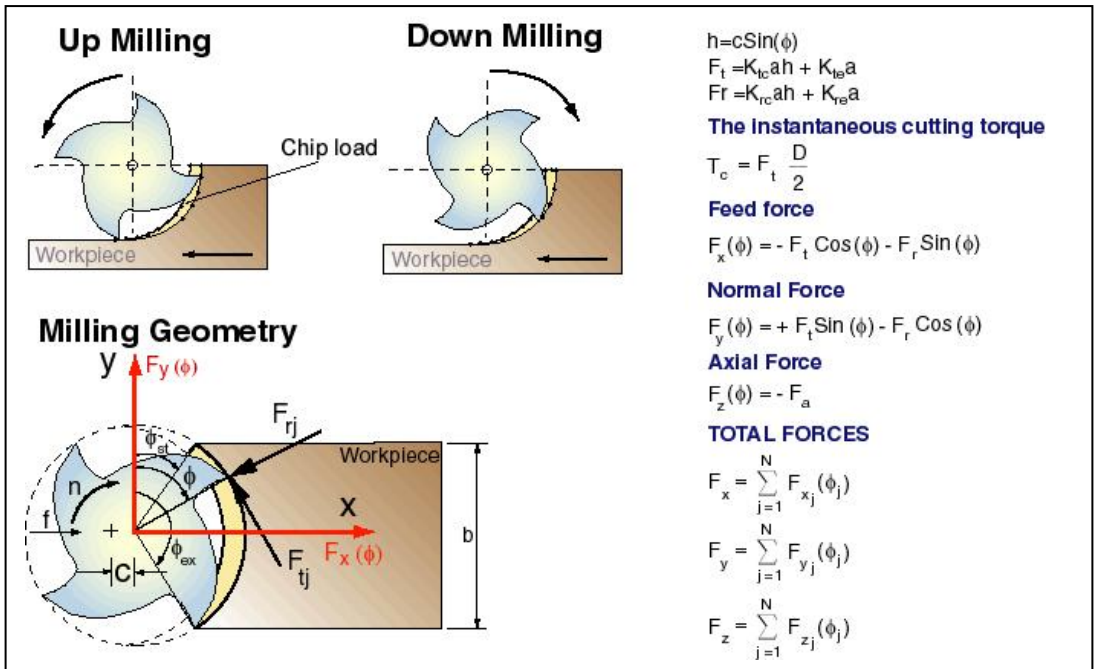

Figure 3 Mechanics of milling [].

$$c(mm/rev/tooth) = \frac{f}{nN}$$

The chip thickness *h(mm)* removed by a single tooth on the cutter when it is at immersion ϕ is expressed from Figure 3 for a cutter with a pitch angle $\phi_p = 2\pi / N$ as :

$$\begin{aligned} &h_j(mm) = c\sin(\phi_j) \quad \leftarrow \phi_j = \phi_0 + j\phi_p \quad , j = 0,1,..,N-1 \\ &if \ \ \phi_j \le \phi_{st} \ \text{or} \ \ \phi_j \ge \phi_{ex} \rightarrow No \ \text{chip} \ h_j(mm) = 0 \end{aligned} \tag{1}$$

The tangential force acting on the tooth is,

$$F_{tj}(\phi) = K_{tc} a h(\phi_j) + K_{te} a = K_{tc} a c \sin(\phi_j) + K_{te} a \tag{2}$$

Where a is the axial depth of cut, and K_{tc} is the tangential shear force coefficient and K_{te} is the tangential edge coefficient which reflects the friction between the flank face and finish surface, and plowing of the rounded cutting edge. The radial cutting $F_{rj}(\phi)$ and axial $F_{zj}(\phi)$ cutting forces can be expressed in a similar manner as,

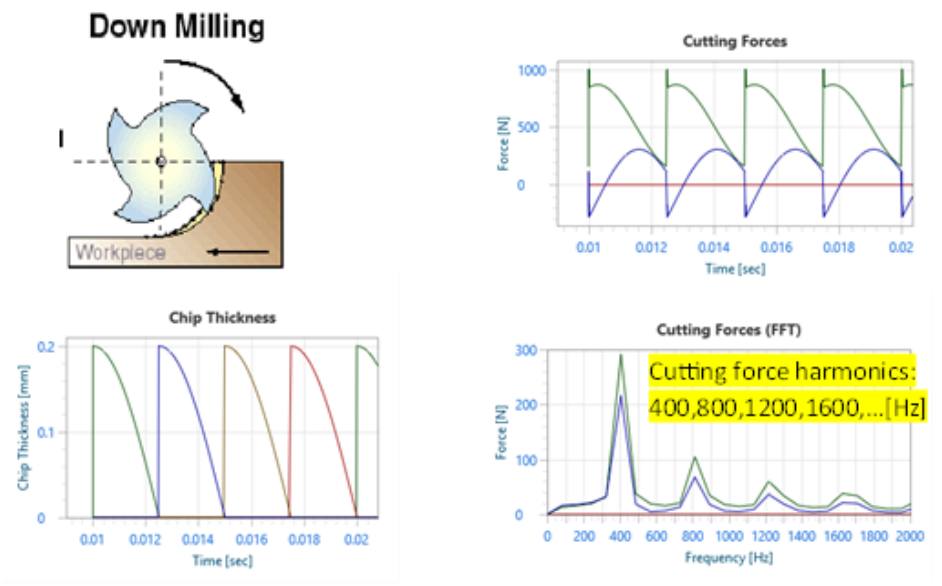

Figure 4 Cutting forces in down milling and frequency spectrum at tooth passing frequency and its harmonics.

$$F_{rj}(\phi_j) = K_{rc} a c \sin(\phi_j) + K_{re} a$$
$$F_{zj}(\phi_j) = K_{zc} a c \sin(\phi_j) + K_{ze} a \quad (3)$$

By projecting the forces in feed (x) and normal (y) for tooth number j ,

$$\begin{aligned} F_{xj}(\phi) &= -F_{tj}(\phi)\cos(\phi_j) - F_{rj}(\phi_j)\sin(\phi_j) \\ &= -\left[K_{tc} a c \sin(\phi_j) + K_{te} a\right]\cos(\phi_j) - \left[K_{rc} a c \sin(\phi_j) + K_{re} a\right]\sin(\phi_j) \\ &= -K_{tc} a c \sin(\phi_j)\cos(\phi_j) - K_{te} a \cos(\phi_j) - K_{rc} a c \sin(\phi_j) - K_{re} a \sin(\phi_j) \\ &= -K_{tc} a c \sin(\phi_j)\cos(\phi_j) - K_{rc} a c \sin(\phi_j) - K_{te} a \cos(\phi_j) - K_{rc} a c \sin(\phi_j) \\ F_{yj}(\phi) &= +F_{tj}(\phi)\sin(\phi_j) - F_{rj}(\phi_j)\cos(\phi_j) \\ &= \left[K_{rc} a c \sin(\phi_j) + K_{re} a\right]\sin(\phi_j) - \left[K_{rc} a c \sin(\phi_j) + K_{re} a\right]\cos(\phi_j) \\ &= K_{rc} a c \sin^2(\phi_j) - K_{rc} a c \sin(\phi_j)\cos(\phi_j) + K_{re} a \sin(\phi_j) - K_{re} a \cos(\phi_j) \end{aligned} \quad (4)$$

The total cutting forces on the cutter can be evaluated by summing the forces contributed by all teeth which are in the cutting zone,

$$F_x(\phi) = \sum_{j=1}^{N} F_{xj}(\phi_j) \ , \ F_y(\phi) = \sum_{j=1}^{N} F_{yj}(\phi_j) \ , F_z(\phi) = \sum_{j=1}^{N} F_{zj}(\phi_j) \quad (5)$$

Torque $T_c(\phi)$ and power $P(\phi)$ on the spindle can be calculated as,

$$T_c(\phi) = \frac{D}{2}\sum_{j=0}^{N-1} F_{tj}(\phi_j)$$
$$P(\phi) = V\sum_{j=0}^{N-1} F_{tj}(\phi_j) \quad \leftarrow V = \pi Dn/60 \tag{6}$$

where D is the cutter diameter and $n(rev/\min)$ is the spindle speed. Sample simulations of cutting forces are shown in Figure 4. The forces are periodic at tooth passing periods, hence their fundamental frequency is equal to tooth passing frequency $\omega_T(Hz) = Nn(rev/\min)/60$ where N is the number of teeth on the cutter and $n(rev/\min)$ is the spindle speed. These periodic cutting forces excite the machine and part structures and cause their vibrations.

The cutting force coefficients for Al7050 are identified as: $K_{tc} = 850\ (N/mm^2) = 850\times10^6 (N/m^2), K_{rc} = 200\times10^6 (N/m^2)$.

It is important to avoid shank breakage of end mills under cutting forces. Let's assume that the maximum resultant force in xy plane of an end mill is $F = \sqrt{F_x^{\,2} + F_y^{\,2}}$ with a diameter D as shown in Figure 5. The bending moment at the end mill–holder interface is: $M = FL$ where L is the stick out of the tool from the holder. The bending stress will be:

$$\sigma = \frac{M}{I}\frac{D}{2} = \frac{FL}{\pi D^4/64}\frac{D}{2} = \frac{32FL}{\pi D^3} \tag{7}$$

Which must be less than the ultimate strength of the carbide $\sigma_{UTS} = 344$ MPa:

$$\sigma < 344MPa \tag{8}$$

The cutting forces are simulated for the selected feed, axial depth, and radial width of cut for all tools and cutting conditions. The maximum bending stress is calculated to be sure that the end mill would not snap at the holder connection.

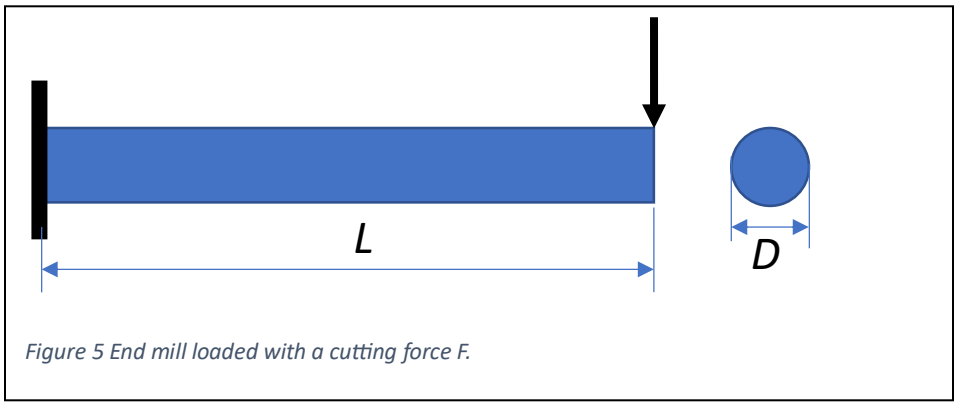

Figure 5 End mill loaded with a cutting force F.

2.2 - Modeling the structural dynamics of machines.

Although machine tools have multiple natural frequencies, the concept of identifying the natural frequency, stiffness and damping properties can be explained by using a single degree of freedom system. The following formulation is taken from the machining course of Dr. Altintas, and it is also explained in his textbook []. If we assume an end mill attached to the spindle is modeled by a spring, damping and mass at the tool tip as shown in Figure 6, the equation of motion at the tool tip is described as:

$$m\frac{d^2x}{dt^2} = -c\frac{dx}{dt} - kx(t) + F(t)$$
$$m\frac{d^2x}{dt^2} + c\frac{dx}{dt} + kx(t) = F(t) \qquad (9)$$

Where m, c, k are the lumped mass, damping and stiffness of the tool at its tip, $F(t)$ is the external force and $x(t)$ is the vibration at the tool tip. The system can be represented in a traditional vibration form as:

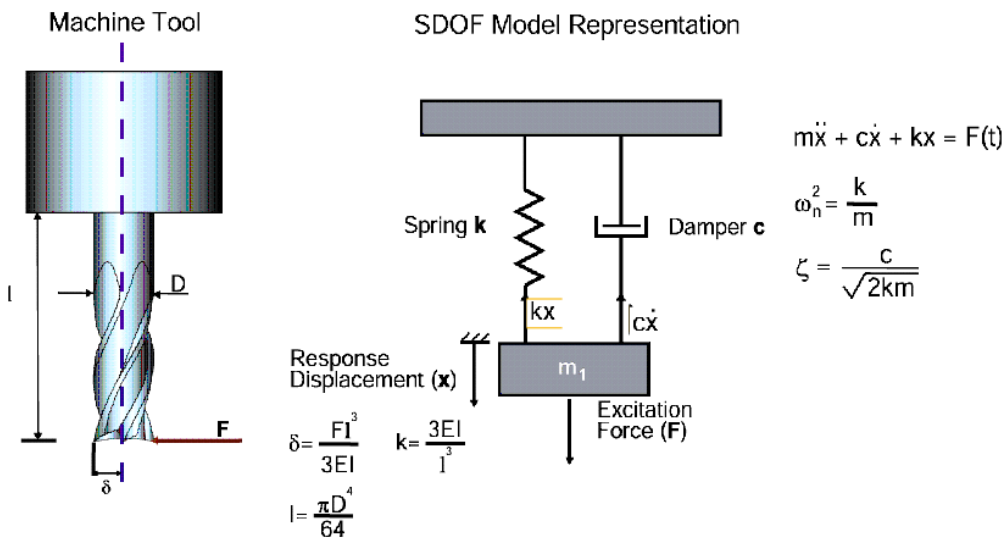

Figure 6 Equation of motion for a single degree of freedom end mill system [2].

$$\frac{d^2x}{dt^2} + \frac{c}{m}\frac{dx}{dt} + \frac{k}{m}x(t) = \frac{1}{m}F(t)$$
$$\frac{d^2x}{dt^2} + 2\zeta\omega_n\frac{dx}{dt} + \omega_n{}^2x(t) = \frac{\omega_n{}^2}{k}F(t) \qquad (10)$$

where $\omega_n(rad/s)=\sqrt{k/m}$ is the natural frequency, $\zeta = c/\sqrt{2km}$ is the dimensionless damping ratio and $k(N/m)$ is the stiffness. Eq. (10) can be expressed in the Laplace domain by taking the Laplace operator $s \equiv d/dt$ as:

$$\begin{aligned} s^2x(s)+2\zeta\omega_n sx(s)+{\omega_n}^2x(s)&=\frac{{\omega_n}^2}{k}F(s) \\ \left(s^2+2\zeta\omega_n s+{\omega_n}^2\right)x(s)&=\frac{{\omega_n}^2}{k}F(s) \end{aligned} \tag{11}$$

The transfer function between the vibration (output) and force (input) for a single degree of freedom system is described as:

$$\Phi(s)=\frac{x(s)}{F(s)}=\frac{{\omega_n}^2/s}{s^2+2\zeta\omega_n s+{\omega_n}^2} \tag{12}$$

By assuming that the input force is sinusoidal, the output vibration will also be sinusoidal in the steady state operation of the machine. Such an assumption leads to the Frequency response of the machine by replacing $s=j\omega$ where $j=\sqrt{-1}$ and ω is the frequency of sinusoidal excitation force.

$$\Phi(s=j\omega)=\frac{x(\omega)}{F(\omega)}=\frac{{\omega_n}^2/s}{(j\omega)^2+j2\zeta\omega_n\omega+{\omega_n}^2}=\frac{{\omega_n}^2/s}{{\omega_n}^2-\omega^2+j2\zeta\omega_n\omega} \tag{13}$$

Where $\Phi(s=j\omega)$ is a complex function called the Frequency Response Function (FRF) of the machine. A complex number can be represented by its real and imaginary parts or by its magnitude and phase as follows (Figure 7):

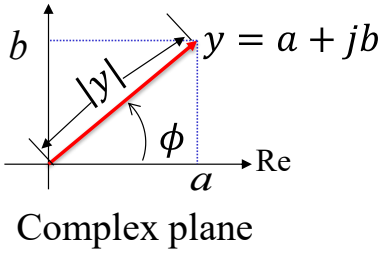

Figure 7 Complex number.

$$y=a+jb \text{ or } |y|=\sqrt{a^2+b^2}\quad \phi=\tan^{-1}\frac{b}{a} \tag{14}$$

Similarly, the complex FRF function of the machine can be represented by its real $G(\omega)$ and imaginary $H(\omega)$ parts as:

$$\Phi(j\omega)=G(\omega)+jH(\omega)$$

$$\text{Real Part}\quad G(\omega)=\frac{{\omega_n}^2}{k}\frac{({\omega_n}^2-\omega^2)}{({\omega_n}^2-\omega^2)^2+(2\varsigma\omega_n\omega)^2} \tag{15}$$

$$\text{Imaginary Part}\quad H(\omega)=-\frac{{\omega_n}^2}{k}\frac{2\varsigma\omega_n\omega}{({\omega_n}^2-\omega^2)^2+(2\varsigma\omega_n\omega)^2}$$

Or by its magnitude and phase:

$$\text{Magnitude } \left|\Phi(\omega)\right| = \sqrt{G^2(\omega) + H^2(\omega)} = \frac{{\omega_n}^2 / k}{\sqrt{\left({\omega_n}^2 - \omega^2\right)^2 + \left(2\zeta\omega_n\omega\right)}} \quad (16)$$

$$\text{Phase} \qquad \phi = \tan^{-1}\frac{H(\omega)}{G(\omega)} = -\tan^{-1}\frac{2\zeta\omega_n\omega}{{\omega_n}^2 - \omega^2}$$

Where the frequency is in [rad/s] and magnitudes are in $[\mu m / N]$. It can be interpreted as follows: When a sinusoidal force is applied with $1N$ force at frequency ω [rad/s], the vibration amplitude will be $\left|\Phi(j\omega)\right|$ [N] and the vibration will follow the force with a time delay of $\omega[rad/s] / \phi[rad]$, i.e. when the force is $F(t) = F\sin(\omega t)$, the vibration becomes $x(t) = F\left|\Phi(\omega)\right|\sin(\omega t - \phi)$. The parameters of the machine ($\omega_n(rad/s), \zeta, k$)are identified experimentally from impact tests as follows. The impact measurement hardware and set up are shown in Figure 8. The hardware consists of a data acquisition box, an impact hammer equipped with a force sensor, and accelerometer to measure the vibrations. The size of the hammer and accelerometer depends on the dimensions of the tool. The smaller the diameter of the tool, smaller the hammer and accelerometer must be to measure the high natural frequencies. Once the tools have been selected, they will then be tap-tested to determine the frequency response of the machine. This is done by attaching an accelerometer to the end of the tool and impacting the opposite end with a modal impulse hammer as shown in Figure 8. Hammer (i.e. input) is connected to channel 1,

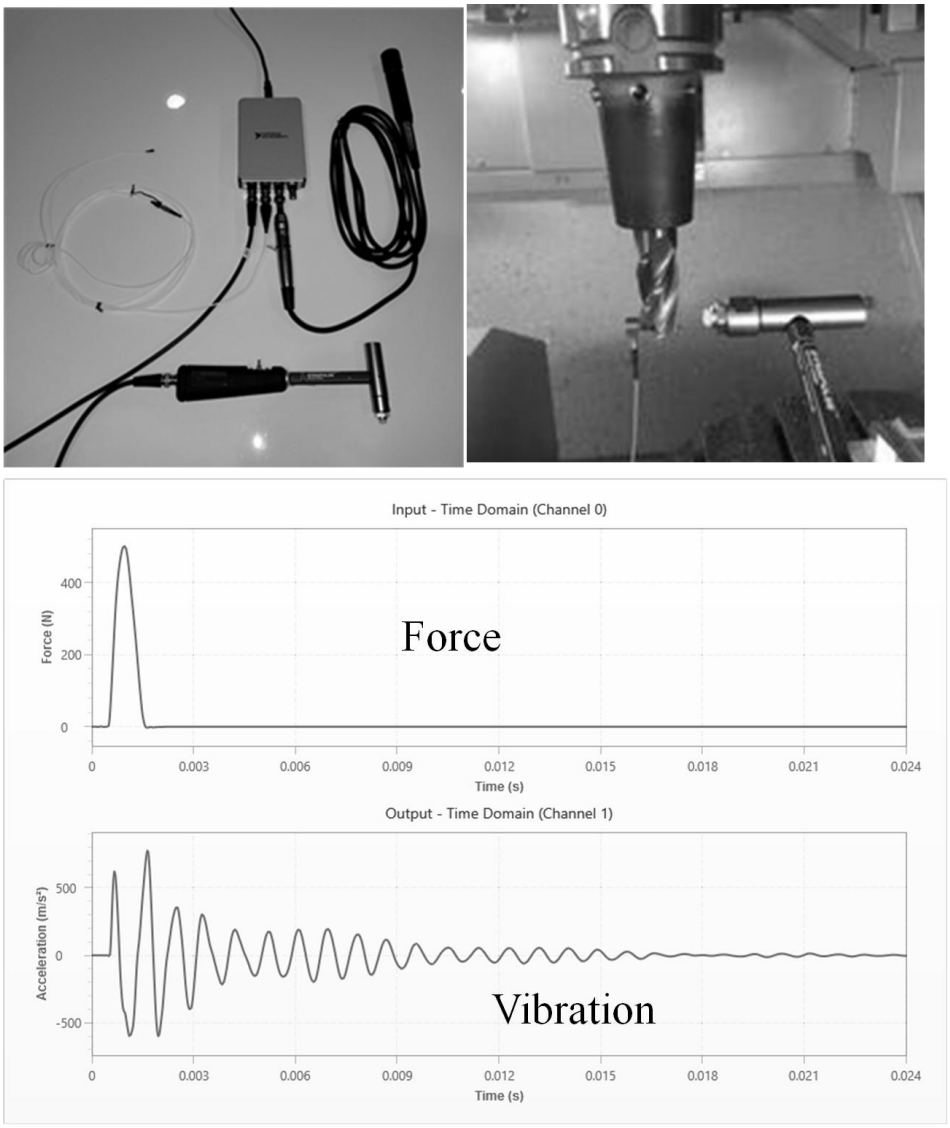

Figure 8 Impact test, applied force and measured vibrations at the tool tip.

and accelerometer (i.e. output) is connected to Channel 2 of the data acquisition system. This measures the so-called Frequency Response Function (FRF) of the machine and tool. The frequency response shows the natural frequencies of the objects measured, which in this case is the machine tool; the DMG MORI DMU 50 with the tool.

Sample FRF 1 is shown in Figure 9. Each peak at the imaginary part represents a structural mode with associated natural frequency, damping ratio and stiffness. The peak at the imaginary part is equal to the approximate formulas, and CUTPRO

software used in the project uses more sophisticated techniques

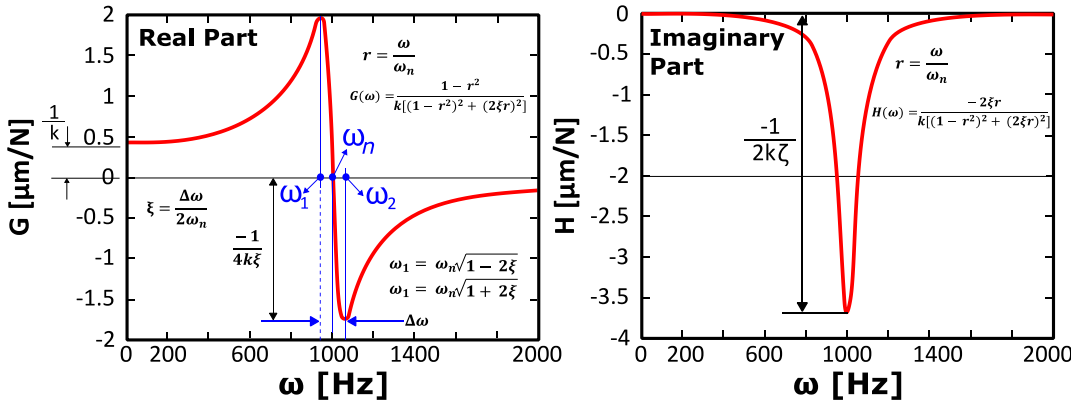

Figure 9 Extraction of modal parameters from FRF measurements.

spindle speed and the number of teeth (N) used in the milling cutter which is called tooth passing frequency $\omega_t[Hz] = Nn/60$ where $n(rev/\min)$ is the spindle speed. In Aluminum machining high spindle speeds are used which means the higher frequencies are being excited (such as the tool). These modes at higher frequencies need to be measured properly to predict the stability of the machine and tool setup accurately.

A sample calculation of modal parameters from the tap test of Tool 1 (Figure 10) is illustrated as follows. The peaks of imaginary parts correspond to natural frequencies and are obtained from the tap test (Figure 10) as,

$$\omega_{n1} = 1289Hz,\ \omega_{n2} = 2996Hz,\ \omega_{n3} = 4238Hz$$

The damping ratios for each mode are,

$$\zeta_1 = \frac{\Delta\omega}{2\omega_n} = \frac{\omega_{21} - \omega_{11}}{2\omega_{n1}} = \frac{1369Hz - 1205Hz}{2(1289Hz)} = \frac{164Hz}{2578Hz} = 6\%$$

$$\zeta_2 = \frac{\Delta\omega}{2\omega_n} = \frac{\omega_{22} - \omega_{12}}{2\omega_{n2}} = \frac{3100Hz - 2800Hz}{2(2996Hz)} = \frac{300Hz}{5992Hz} = 5\%$$

$$\zeta_3 = \frac{\Delta\omega}{2\omega_n} = \frac{\omega_{23} - \omega_{13}}{2\omega_{n3}} = \frac{4309Hz - 3980Hz}{2(4238Hz)} = \frac{329Hz}{8476Hz} = 4\%$$

The stiffnesses of modes are evaluated as,

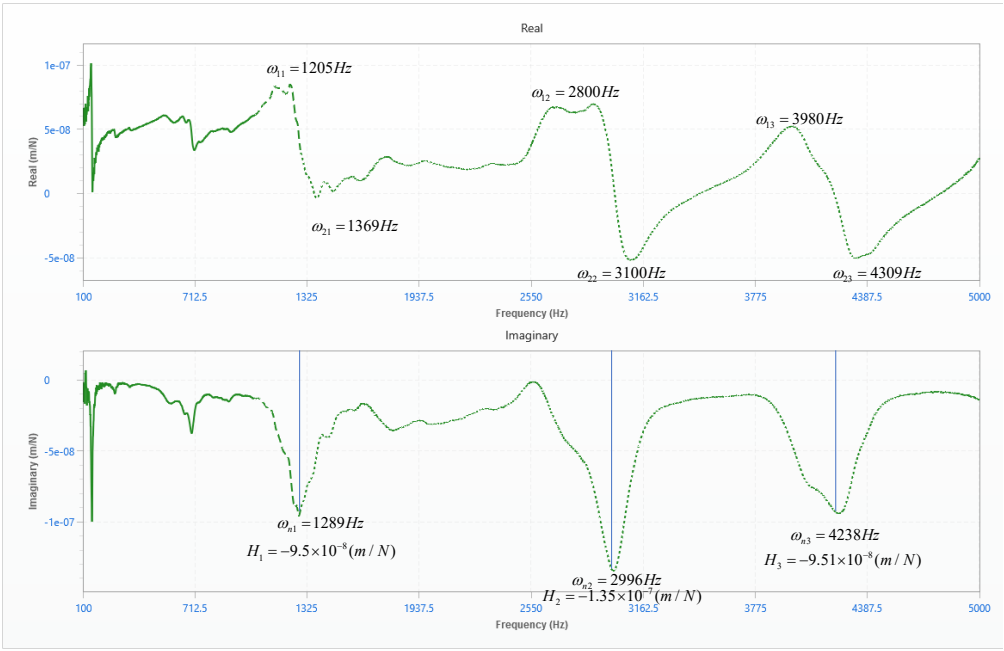

Figure 10 Sample FRF measurement for Tool 1.

$$k_1 = \frac{-1}{2H_1\zeta_1} = \frac{-1}{2(-9.5\times10^{-8})(0.06362)} = 82.73\times10^6\left(N/m\right)$$

$$k_2 = \frac{-1}{2H_2\zeta_2} = \frac{-1}{2(-1.35\times10^{-7})(0.05007)} = 73.97\times10^6\left(N/m\right)$$

$$k_3 = \frac{-1}{2H_3\zeta_3} = \frac{-1}{2(-9.51\times10^{-8})(0.03882)} = 135.44\times10^6\left(N/m\right)$$

These manually calculated modal parameters are close to the values estimated by advanced CUTPRO modal analysis software shown in Table 2. The FRF measurements and identified modal parameters of all 4 tools with CUTPRO Modal Analysis module are given in Table 2, Table 3, Table 4 and Table 5.

Table 2 Identified modal parameters of Tool 1 by CUTPRO modal analysis module.

Mode	$\omega_n(Hz)$	Damping (%)	Modal Stiffness (N/m)
1	1275	7.9	70.8E06
2	3017	3.28	126E06
3	4272	3.46	170E6

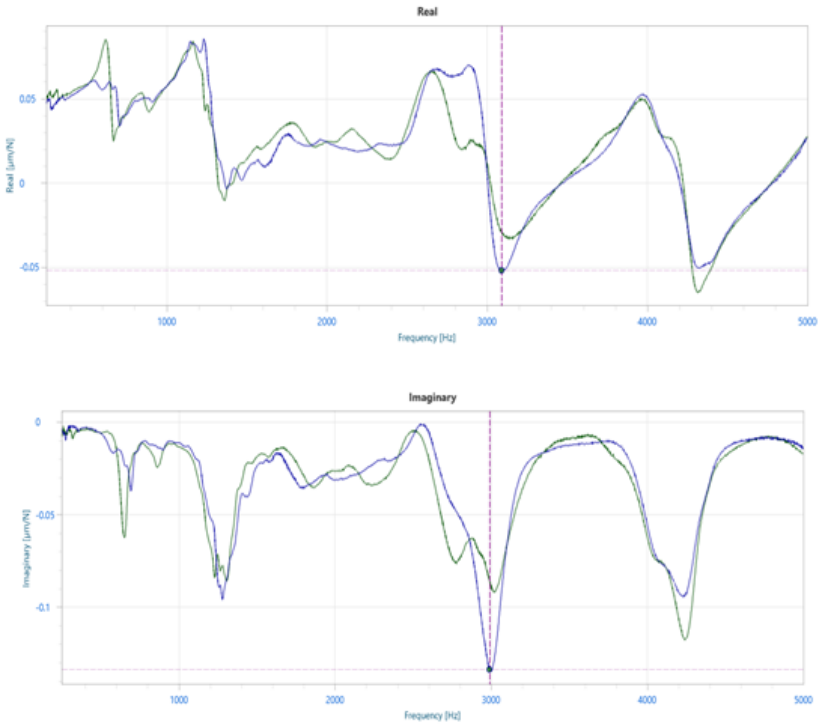

Measured FRF of Tool 2 in X and Y directions

Table 3 Identified modal parameters of Tool 2 by CUTPRO modal analysis module.

Mode	$\omega_n(Hz)$	Damping (%)	Modal Stiffness (N/m)
1	2836	1.77	70.44E06
2	4137	2.54	76.81E06
3	4865	1.53	98.64E06

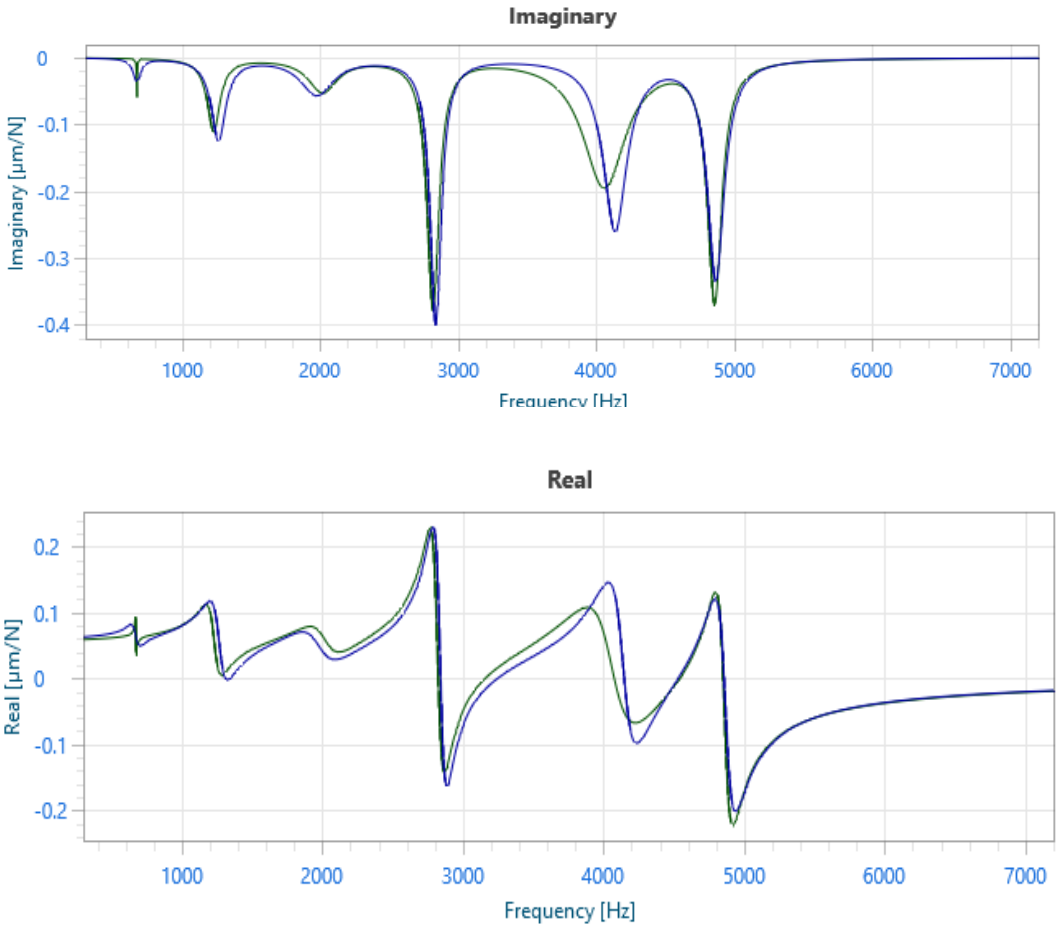

Measured FRF of Tool 2 in X and Y directions

Table 4 Identified modal parameters of Tool 3 by CUTPRO modal analysis module.

Mode	$\omega_n(Hz)$	Damping (%)	Modal Stiffness (N/m)
1	3033	2.67	9.76E06
2	3591	3.41	11.7E06
3	4729	1.74	279E06

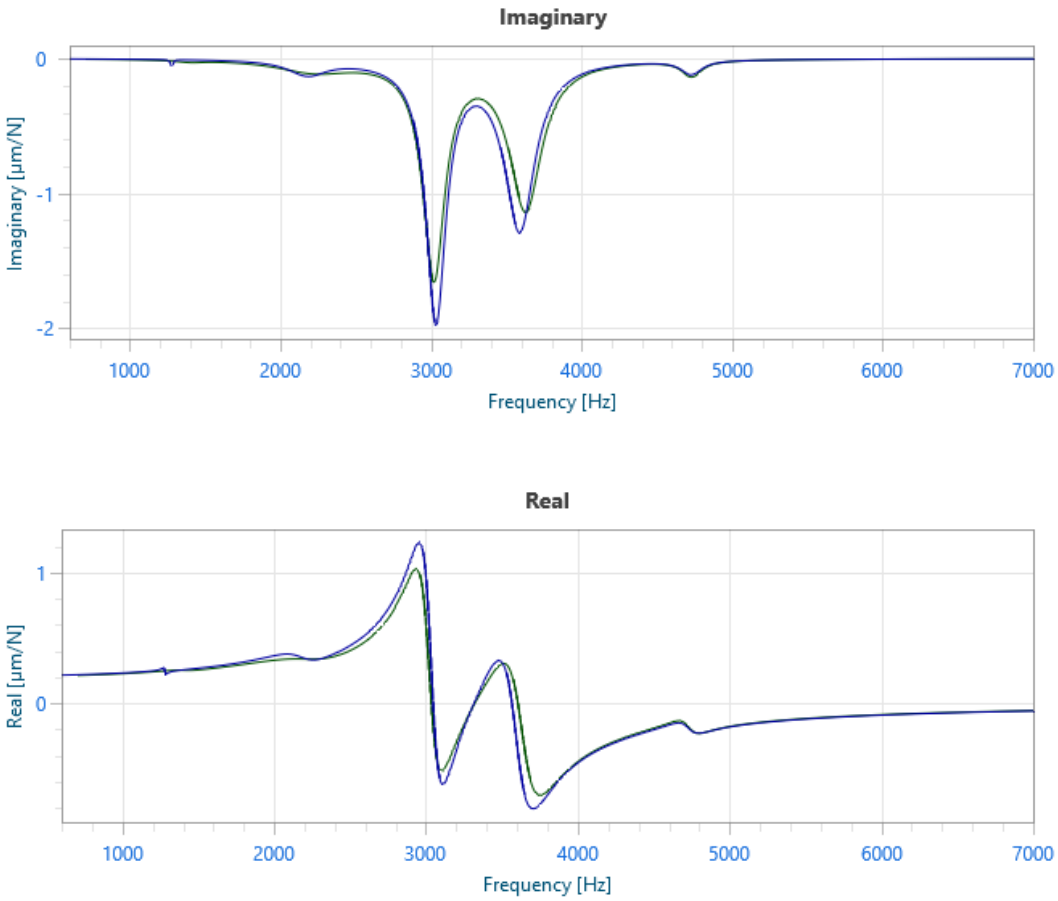

Measured FRF of Tool 3 in X and Y directions.

Table 5 Identified modal parameters of Tool 4 by CUTPRO modal analysis module

Mode	$\omega_n(Hz)$	Damping (%)	**Modal Stiffness (N/m)**
1	2975	2.48	36E06
2	4155	3.51	15.7E06
3	4700	2.36	33.2E06

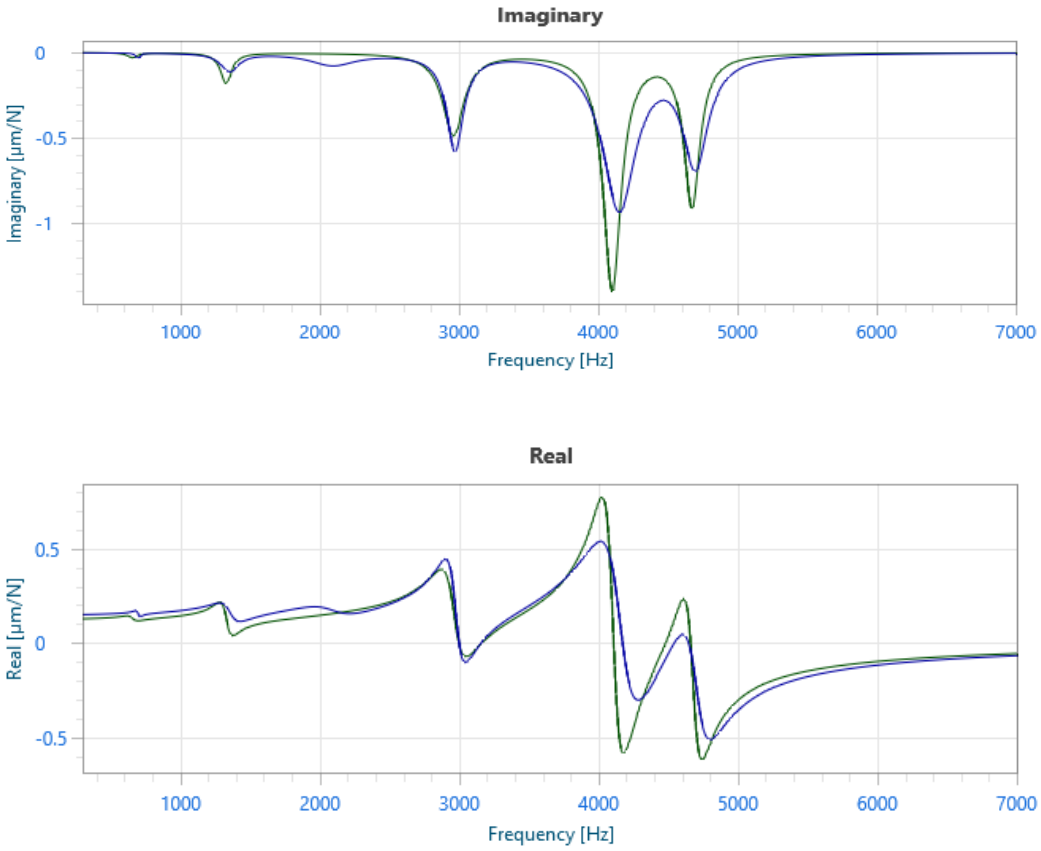

Measured FRF of Tool 4 in X and Y directions.

Chapter 3 - Chatter Stability of Cutting

While plunge turning with a flat cutting edge is considered as an orthogonal cutting operation, most practical machining operations have inclined cutting edges which make the process oblique with cutting forces in all three directions. Also, the cutting operations are classified as single-point machining such as turning and boring with one cutting edge, operations with multiple cutting edges such as milling are considered multi-point machining systems. Chatter stability for a single-point machining operation is called one-dimensional, and multipoint machining has multidimensional chatter stability. Chatter stability for a single point, one-dimensional chatter stability is presented first followed by chatter stability of milling operations. The objective is explained in Figure 11. The FRF of the machine is measured, its modal parameters are identified, chatter-free cutting conditions are identified and used in CAM programming of the part.

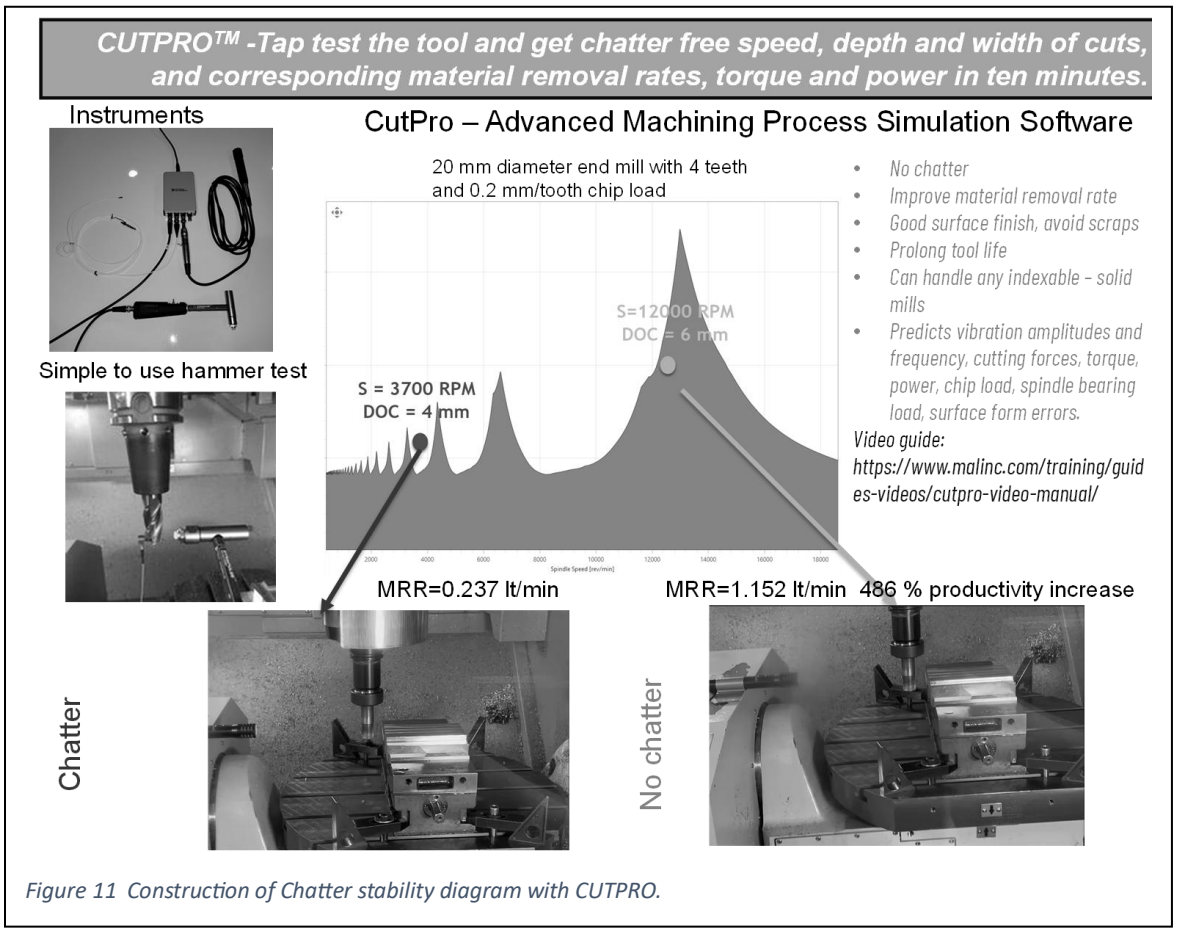

Figure 11 Construction of Chatter stability diagram with CUTPRO.

3.1- Chatter Stability of single point, orthogonal cutting operations

The flat-faced tool is fed through the disc at a feedrate of h_o (mm/rev), hence if there is no vibration, the chip thickness will be h_o as shown in. However, the shaft is flexible with stiffness $k_y(N/m)$, lumped mass $m(kg)$ of the disc and shaft at the cutting point, and the damping constant $c_y(N/m/s)$. When tool touches the disk, it will vibrate $y(t)$ amount of time $t(\mathrm{s})$. If the vibrations did not diminish one spindle period $T(s) = 60/n$, the vibration marks left on the disk during the previous revolution is $y(t-T)$. The resulting dynamic chip thickness becomes:

$$h(t) = h_0 - y(t) + y(t-T) \tag{17}$$

The feed force is then characterized as:

$$F_f(t) = K_f a[h_o + y(t-T) - y(t)]$$

Where a is the radial width of cut, and K_f is radial cutting force coefficient. The radial cutting force F_f is applied on the structural dynamics of the turning system as:

$$m_y\ddot{y}(t) + c_y\dot{y}(t) + k_y y(t) = F_f(t) = K_f a[h_o + y(t-T) - y(t)] \tag{18}$$

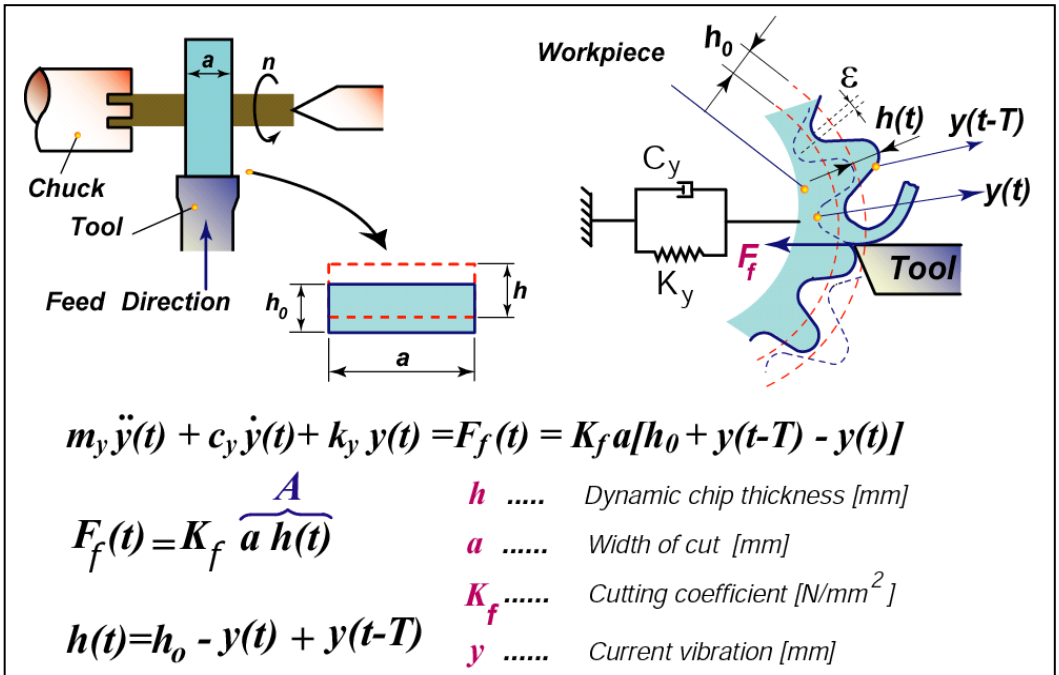

Figure 12 Chatter stability of orthogonal, one dimensional cutting.

The equation can be expressed also as,

$$\ddot{y}(t)+\frac{c_y}{m_y}\dot{y}(t)+\frac{k_y}{m_y}y(t)=\frac{1}{m_y}K_f a[h_o+y(t-T)-y(t)]$$

$$\ddot{y}(t)+2\zeta\omega_n\dot{y}(t)+\omega_n^2 y(t)=F_y(t)=\frac{\omega_n^2}{k_y}K_f a[h_o+y(t-T)-y(t)]$$

(19)

Where ω_n, ζ, k_y are the natural frequency, damping ratio and stiffness of the single degree of freedom turning system shown in Figure 11. The transfer function between the vibrations and force becomes,

$$\Phi(s)=\frac{y(s)}{F_y(s)}=\frac{\omega_n^2/k_y}{s^2+2\zeta\omega_n s+\omega_n^2}\rightarrow y(s)=\Phi(s)F_y(s) \quad (20)$$

The dynamic chip thickness can be expressed in Laplace domain as

$$h(t)=h_0-\left[y(t)-y(t-T)\right]\rightarrow h(s)=h_0-\left[y(s)-e^{-sT}y(s)\right]=h_0-\left(1-e^{-sT}\right)y(s)$$

(21)

By substituting $y(s) = \Phi(s)F_y(s)$ from Eq. (20) into Eq. (21) leads to:

$$h(s) = h_0 - \left[1 - e^{-sT}\right] y(s) = h_0 - \left(1 - e^{-sT}\right)\Phi(s)F(s) = h_0 - \left(1 - e^{-sT}\right)\Phi(s)K_f a h(s) \quad (22)$$

The transfer function $\Phi_c(s)$ between the actual dynamic chip thickness h_d and input chip thickness or feedrate h_0 becomes:

$$\left[1 + \left(1 - e^{-sT}\right)\Phi(s)K_f a\right] h(s) = h_0 \rightarrow \Phi_c(s) = \frac{h(s)}{h_0(s)} = \frac{1}{1 + \left(1 - e^{-sT}\right)\Phi(s)K_f a} \quad (23)$$

The chatter stability of system is governed by the roots of the denominator (i.e. characteristic equation),

$$1 + \left(1 - e^{-sT}\right)\Phi(s)K_f a = 0 \quad (24)$$

Which has infinite number of roots due to exponential delay e^{-sT}. For example, if we open e^{-sT} in Taylor series as $e^{-sT} = 1 - aT + \frac{1}{2}(aT)^2 - \frac{1}{3}(aT)^3 + \ldots.$, there will be infinite roots of Eq. (24) as:

$$1 + \left(1 - e^{-sT}\right)\Phi(s)K_f a = (s - p_1)(s - p_2)(s - p_3).....(s - p_\infty) = 0 \quad (25)$$

Each root can have a complex number as,

$$p = \sigma + j\omega_c \quad (26)$$

The vibrations will contain an exponential term reflecting each root as:

$$y(t) = Y_1 e^{p_1 t} + Y_2 e^{p_1 t} + \ldots + Y_\infty e^{p_\infty t} \quad (27)$$

If any of the root has a positive real part $\sigma > 0$, the vibrations will exponentially grow theoretically to infinity $t \rightarrow \infty$ then $Y_1 e^{\sigma t} e^{j\omega_c t} = \rightarrow \infty$ because $e^{\sigma t} = e^{\infty t} = \infty$ which means chatter. In summary,

$$\begin{aligned}
&1 + \left[G + jH - \left(G\cos\omega_c T - jG\sin\omega_c T + jH\cos\omega_c T + H\sin\omega_c T\right)\right] K_f a = 0 \\
&1 + \left[G + jH - G\cos\omega_c T + jG\sin\omega_c T - jH\cos\omega_c T - H\sin\omega_c T\right] K_f a = 0 \\
&\left\{1 + K_f a\left[G\left(1 - \cos\omega_c T\right) - H\sin\omega_c T\right]\right\} + jK_f a\left[H\left(1 - \cos\omega_c T\right) + G\sin\omega_c T\right] = 0
\end{aligned} \quad (28)$$

$$\begin{aligned}&\sigma > 0; unstable - chatter\\&\sigma < 0; stable - nochatter\\&\sigma = 0, s = j\omega_c; criticallystable\end{aligned} \quad (29)$$

Tlusty and Tobias independently developed the following orthogonal chatter stability theory. For a critically stable system $s = j\omega_c$ is substituted in the characteristic equation as:

$$s = j\omega_c \rightarrow 1 + \left(1 - e^{-sT}\right)\Phi(s)K_f a = 0 \rightarrow 1 + \left(1 - e^{-j\omega_c T}\right)\Phi(j\omega_c)K_f a = 0 \quad (30)$$

By substituting $e^{-j\omega_c T} = \cos\omega_c T - \sin\omega_c T$ and $\Phi(j\omega_c) = G(\omega_c) + jH(\omega_c)$ Eq. (30) becomes,

$$\begin{aligned}&1 + \left[1 - \left(\cos\omega_c T - j\sin\omega_c T\right)\left(G(\omega_c) + jH(\omega_c)\right)\right]K_f a\\&= 1 + \left[1 - \left(\cos\omega_c T - j\sin\omega_c T\right)\left(G + jH\right)\right]K_f a = 0\end{aligned} \quad (31)$$

By separating real and imaginary parts of Eq. (31),

$$\begin{aligned}&1 + \left[G + jH - \left(G\cos\omega_c T - jG\sin\omega_c T + jH\cos\omega_c T + H\sin\omega_c T\right)\right]K_f a = 0\\&1 + \left[G + jH - G\cos\omega_c T + jG\sin\omega_c T - jH\cos\omega_c T - H\sin\omega_c T\right]K_f a = 0\\&\underbrace{\left\{1 + K_f a\left[G\left(1 - \cos\omega_c T\right) - H\sin\omega_c T\right]\right\}}_{Real} + j\underbrace{K_f a\left[H\left(1 - \cos\omega_c T\right) + G\sin\omega_c T\right]}_{Imaginary} = 0\end{aligned} \quad (32)$$

Both real and imaginary parts of Eq. (32) must be zero to find the critical depth of cut $a_{\lim}$ and corresponding spindle period T.

$$\begin{aligned}1 + K_f a\left[G\left(1 - \cos\omega_c T\right) - H\sin\omega_c T\right] = 0\\K_f a\left[H\left(1 - \cos\omega_c T\right) + G\sin\omega_c T\right] = 0\end{aligned} \quad (33)$$

If we consider the imaginary part first,

$$\begin{aligned}&\left[H\left(\omega_c\right)\left(1 - \cos\omega_c T\right) + G\left(\omega_c\right)\sin\omega_c T\right] = 0\\&G\left(\omega_c\right)\sin\omega_c T = H\left(\omega_c\right)\left(\cos\omega_c T - 1\right) \rightarrow \frac{H\left(\omega_c\right)}{G\left(\omega_c\right)} = \frac{\sin\omega_c T}{\cos\omega_c T - 1} = \tan\psi(\omega_c)\end{aligned} \quad (34)$$

$G\left(\omega_c\right), H\left(\omega_c\right)$ are the real and imaginary parts of FRF and $\psi(\omega_c)$ is the phase of FRF at the chatter frequency ω_c when the process is at critically stable depth of cut $a_{\lim}$ and speed speed $n = 60/T$. By using the following trigonometric relationships,

$$\sin\omega_c T = 2\sin\frac{\omega_c T}{2}\cos\frac{\omega_c T}{2} \text{ and } \cos\frac{\omega_c T}{2} = \cos^2\frac{\omega_c T}{2} - \sin^2\frac{\omega_c T}{2}$$

Eq. (34) can be transformed to:

$$\tan\psi(\omega_c) = \frac{H(\omega_c)}{G(\omega_c)} = \frac{\sin\omega_c T}{\cos\omega_c T - 1}$$
$$= \frac{2\sin\frac{\omega_c T}{2}\cos\frac{\omega_c T}{2}}{\cos^2\frac{\omega_c T}{2} - \sin^2\frac{\omega_c T}{2} - \sin^2\frac{\omega_c T}{2} - \cos^2\frac{\omega_c T}{2}} = \frac{\cos\frac{\omega_c T}{2}}{-\sin\frac{\omega_c T}{2}}$$
$$\tan\psi(\omega_c) = \tan\left(\frac{\omega_c T}{2} - \frac{3\pi}{2}\right) \rightarrow \psi(\omega_c) = \frac{\omega_c T}{2} - \frac{3\pi}{2}$$

(35)

Which can be arranged as,

$$\omega_c T = 2\psi + 3\pi = \varepsilon + k2\pi \leftarrow \varepsilon = 2\psi + \pi,\ k = 1,2,3,... \quad (36)$$

Where k represents the number of roots or *lobes* we consider in characteristic equation. The spindle speed can be evaluated as,

$$T[s] = \frac{3\pi + 2\psi}{\omega_c(rad/s)} = \frac{k2\pi + \varepsilon}{\omega_c(rad/s)}, \quad \leftarrow \{\varepsilon = 2\psi + \pi\ , \psi(\omega_c) = \tan^{-1}\frac{H(\omega_c)}{G(\omega_c)}\}$$
$$n(rev/\min) = \frac{60}{T}$$

(37)

Where phase angle $\psi(\omega_c)$ is found from the measured FRF of the structure.

If we consider the real part as well,

$$1 + K_f a\left[G\left(1-\cos\omega_c T\right) - H\sin\omega_c T\right] = 0 \quad (38)$$

By pulling the depth of cut and calling it limit or critical depth of cut $a_{\lim}$,

$$a_{\lim} = -\frac{1}{K_f\left[G\left(1-\cos\omega_c T\right) - H\sin\omega_c T\right]} = -\frac{1}{GK_f\left[\left(1-\cos\omega_c T\right) - \frac{H}{G}\sin\omega_c T\right]}$$

(39)

By substituting $\frac{H(\omega_c)}{G(\omega_c)} = \frac{\sin\omega_c T}{\cos\omega_c T - 1}$ from Eq. (34),

$$a_{\lim} = -\frac{1}{GK_f\left[\left(1-\cos\omega_c T\right)+\frac{\sin\omega_c T}{1-\cos\omega_c T}\sin\omega_c T\right]} = -\frac{1}{GK_f\left[\frac{\left(1-\cos\omega_c T\right)^2+\sin^2\omega_c T}{1-\cos\omega_c T}\right]}$$

$$a_{\lim} = -\frac{1}{GK_f\left[\frac{1-2\cos\omega_c T+\cos^2\omega_c T+\sin^2\omega_c T}{1-\cos\omega_c T}\right]} = -\frac{1}{2GK_f\left[\frac{1-\cos\omega_c T}{1-\cos\omega_c T}\right]}$$

(40)

The critical depth of cut becomes,

$$\text{Depth of cut } a_{\lim} = -\frac{1}{2G(\omega_c)K_f} \tag{41}$$

The stability charts can be calculated by selecting frequencies from FRF with negative real part and calculating the critical depth of cut $a_{\lim} = -\frac{1}{2G(\omega_c)K_f}$ and corresponding spindle speed as at each frequency ω_c as

$T[s] = \frac{3\pi + 2\psi}{\omega_c(rad/s)} = \frac{k2\pi + \varepsilon}{\omega_c(rad/s)}$, and $\varepsilon = 2\psi + \pi$, $n(rev/\min) = \frac{60}{T}$ where $\psi(\omega_c) = \tan^{-1}\frac{H(\omega_c)}{G(\omega_c)}$.

Each frequency in FRF file is used if its real part $G(\omega_c) < 0$, and k can be increased to cover the speed range of the machine tool. It must be noted that when the spindle speed is very close to the natural frequency of the machine, the depth of cut becomes maximum,

$$a_{\lim} = -\frac{1}{2K_{\lim}G_{\min}(1.00001\omega_n)} = +\infty \text{ and } G_{\min}(1.00001\omega_n) \approx -0 \tag{42}$$

In short, the machine must be rotated at a speed close to the natural frequency of the machine to create almost a resonance which will lead to highest material removal rate hence the productivity. This is the concept behind the invention of high-speed spindles by Tlusty.

Tlusty modified Eq. (41) to apply it to milling by adding a correction factor m_e as shown in Figure 13,

$$a_{\lim} = -\frac{1}{2G(\omega_c)K_f m_e} \leftarrow m_e = \frac{N}{2}\frac{b}{D} \tag{43}$$

where b is the radial width of cut, D is the end mill diameter and N is the number of teeth on the cutter.

A sample stability calculation is presented below for an illustration of the procedure. The cutting force coefficients for Aluminum 7050 are identified as: The cutting force coefficients for Al7050 are identified as: $K_{tc} = 850\ (N/mm^2) = 850\times10^6 (N/m^2), K_{rc} = 200\times10^6 (N/m^2)$.

The frequency (ω_c), real part $(G(\omega_c))$ and imaginary part $(H(\omega_c))$ are read from the FRF measurement of Tool 2 from Table 2. The tool has $N = 5$ teeth and slot milling case ($b = D$) is considered, hence $m_e = \frac{b}{D}\frac{5}{2} = \frac{5}{2} = 2.5$. The stability equation for milling becomes,

$$a_{\lim} = -\frac{1}{2G(\omega_c)K_f m_e} = \frac{1}{2G(\omega_c)\times 850E6\times 2.5}$$

$$\psi = \tan^{-1}\frac{H(\omega_c)}{G(\omega_c)}, \quad \varepsilon = 2\psi + \pi$$

$$\text{Tooth period } T[s] = \frac{3\pi + 2\psi}{\omega_c(rad/s)} = \frac{k2\pi + \varepsilon}{\omega_c(rad/s)}$$

$$\text{Spindle speed } n(rev/\min) = \frac{60}{NT} = \frac{60}{5T}$$

The stability is calculated using Tlusty's stability theory is shown as follows:

- Select a frequency from FRF where $G(\omega)$ is negative to get positive depth of cut in Eq. (43)
- Read the values of $G(\omega), H(\omega)$ from FRF
- Calculate limit depth of cut using Eq. (43)

$$a_{\lim} = -\frac{1}{2G(\omega_c)K_f m_e} \leftarrow m_e = \frac{N}{2}\frac{b}{D}$$

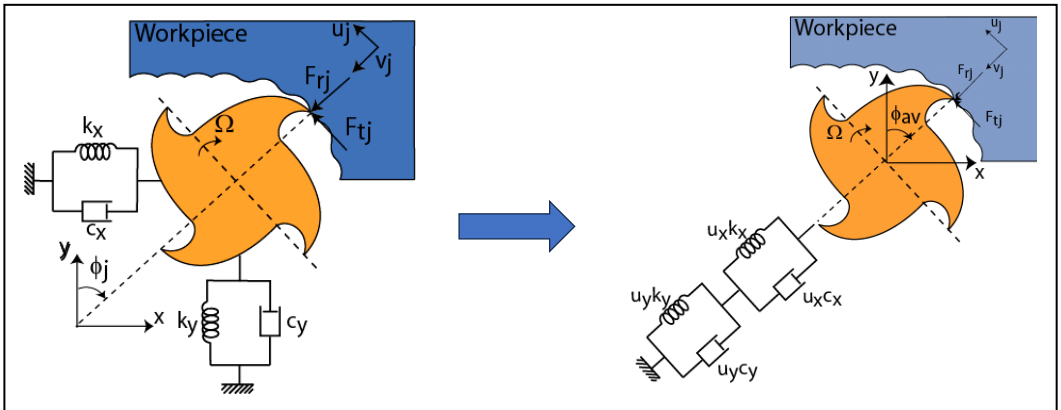

Figure 13 Approximation of milling to use Tlusty's theory [1].

- Calculate the phase $\psi = \tan^{-1}\frac{H(\omega_c)}{G(\omega_c)}$ and $\varepsilon = 2\psi + \pi$
- Vary the number of lobes $k = 1, 2, ..20$ and calculate the tooth period for each k: Tooth period $T[s] = \frac{3\pi + 2\psi}{\omega_c(rad/s)} = \frac{k2\pi + \varepsilon}{\omega_c(rad/s)}$
- Calculate the spindle speed $n(rev/\min) = \frac{60}{NT}$
- Scan all frequencies where $G(\omega)$ is negative and repeat.

A sample calculation for one frequency is shown in Figure 14.

ω_c (Hz)	$G(\omega_c)$ xE-6	$H(\omega_c)$ xE-6	$a_{lim}(m)$= $-1/(2K_{tc}G)$	ψ(rad)= $\tan^{-1}$(H/G)	ϵ(rad)= $2\psi + \pi$	k	T[sec]= $(2\pi k+\epsilon)/2\pi\omega$	n(rev/ min)= 60/T
2895	-0.0055	-0.133	1/(2*850 E6*5.534E-09) = 24.5 E-6	23.82214216	50.78	1	57.07/18918.7 =0.003016547	19890
						2	63.35/18918.7 =0.003348538	17918
						3	69.63/18918.7 =0.003680772	16301
						.		

Figure 14 Construction of stability diagrams.

Using MATLAB a simple stability program has been written using Tlusty's stability lobes. The values of ω_n ζ and k are read from the FRF plot and used to calculate the stability. A MATLAB program to calculate chatter stability using Tlusty's approximation is given in Appendix A, and the results are given in Figure 15. The selected speed and depth of cut must be selected below the diagrams. By considering the tool holder manufacturer's balancing rules, the axial depth of cut of $a_{\lim} = 1mm$ and spindle speed of 11,500 rev/min is used.

The stability is also calculated using CUTPRO Advanced Machining Software which uses more accurate but complex theory [1][3] as shown in Figure 19. While my calculation shows about

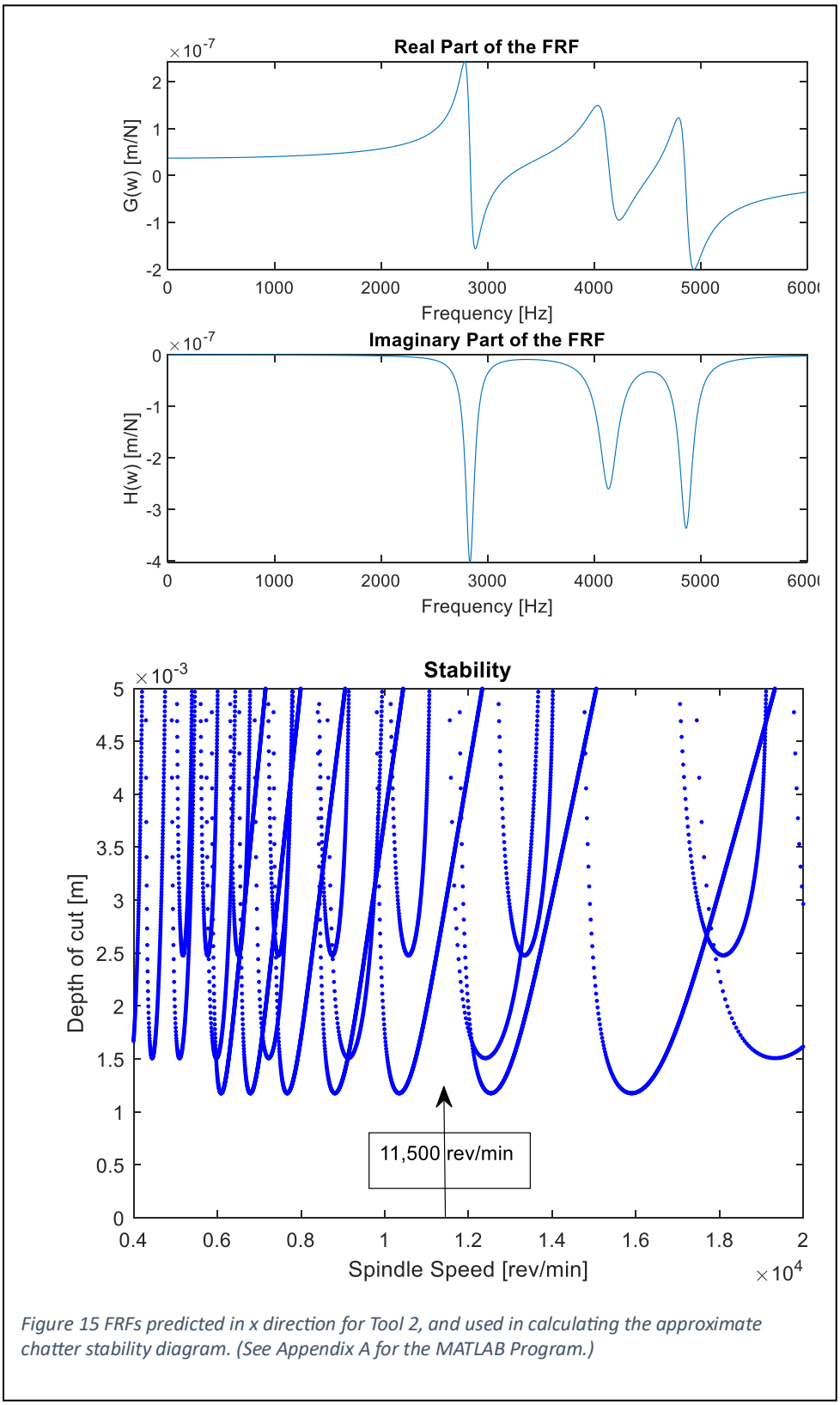

Figure 15 FRFs predicted in x direction for Tool 2, and used in calculating the approximate chatter stability diagram. (See Appendix A for the MATLAB Program.)

1.2mm minimum depth of cut for all speeds (Figure 15), CUTPRO gives about 0.9mm depth of cut (Figure 19), but both show stable pocket at 11,500 rev/min. CUTPRO results are also tested on the machine as shown in Figure 19, and adopted in preparing NC part program.

The chip shapes are shown in Figure 16. When the depth of cut is way below a minimum depth of cut, there is hardly any vibration, but the productivity is low. When the depth of cut and speed are selected above the stability, the machine chatters, and the waves on both sides of the chip are not parallel and they grow, so as the force which is called chatter. When the speed is selected at the stability pocket, i.e. 11,500 rev/min in Figure 19, the machine resonates, and leaves forced vibrations, but the waves are parallel to each other and chip thickness is the same hence the load on the machine does not grow. Henceforth, CUTPRO stability results are used to prepare the NC Part program.

3.4 - Stability and Cutting Condition Selection using CUTPRO

The cutting conditions are selected from the tap tests and chatter stability diagrams. The goal is to obtain chatter-free cutting conditions with high MRR. CUTPRO software is used to simulate the machine tool cutting metal with the tap tests containing the frequency response of the machine and tool.

Some test cuts need to be made to verify the stability lobe accuracy in case mistakes were made during the tap test measurement. Sometimes the stability can have inaccuracies if the tap tests were not conducted well, or the spindle of the machine behave differently during rotation, i.e. spindle bearing pre-loads can be altered in high-speed machining (high RPMs).

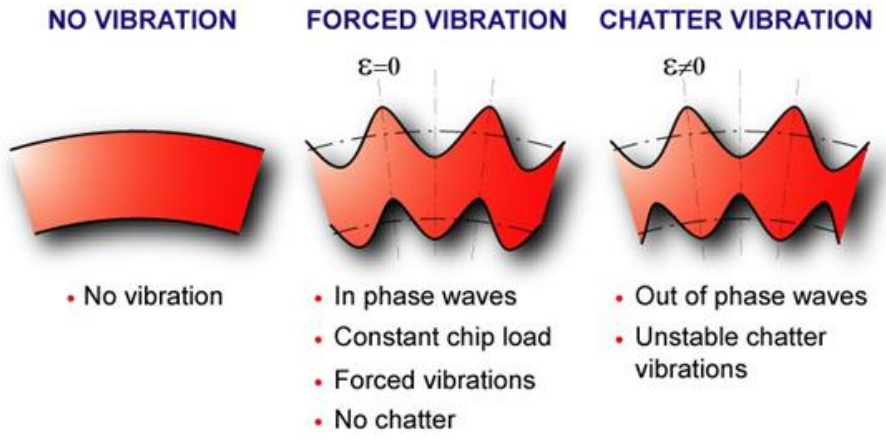

Figure 16 Chip shapes during machining

Tool 1 stability and experimental verifications are given in Figure 17. All tests were chatter-free free as predicted. The serrated roughing tool with 20 mm diameter and 4 teeth is used at 9180 rev/min, 36 mm axial depth of cut and 10 mm radial depth in down milling. The simulated cutting forces for this condition is given in Figure 18, where the

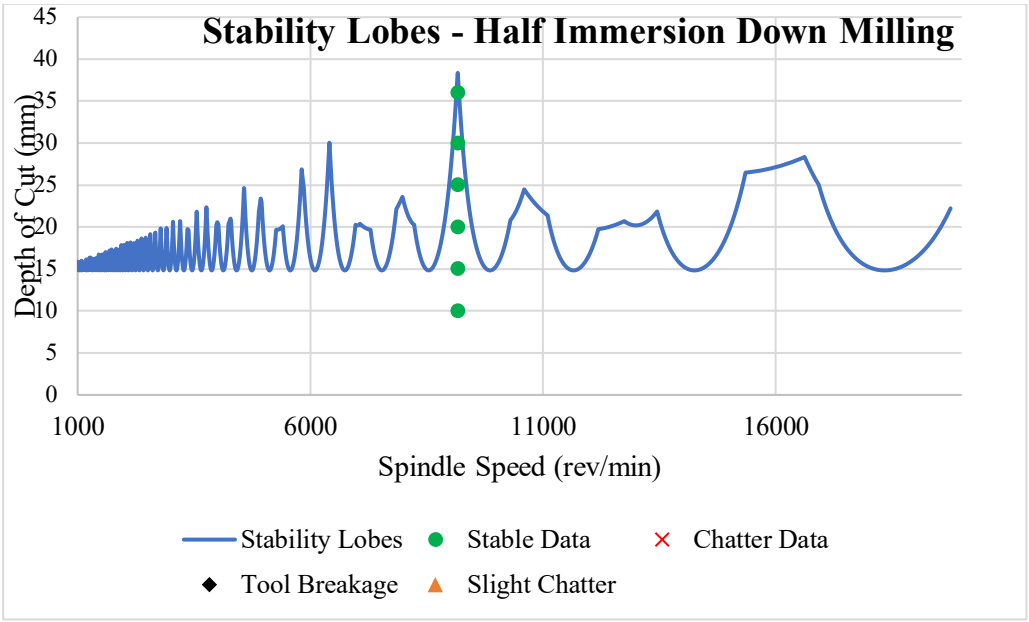

Tool 1 - Stability

Test Number	n [rpm]	a_p [mm]	a_e [mm]	c [mm/rev/tooth]	Condition
1	9180	10	10	0.1	Stable
2	9180	15	10	0.1	Stable
3	9180	20	10	0.1	Stable
4	9180	25	10	0.1	Stable
5	9180	30	10	0.1	Stable
6	9180	36	10	0.1	Stable

Figure 17 Tool 1 stability from CUTPRO. Serrated end mill with 20 mm diameter and four flutes.

maximum force is 4000N. The resulting bending stress at the holder interface is (Eq. (7)),

$\sigma = \frac{32FL}{\pi D^3} = \frac{32 \times 4000 \times 55.6}{\pi (20)^3} = 283MPa < 344MPa$ and it is less than the Ultimate strength of carbide tool hence the tool will not be broken.

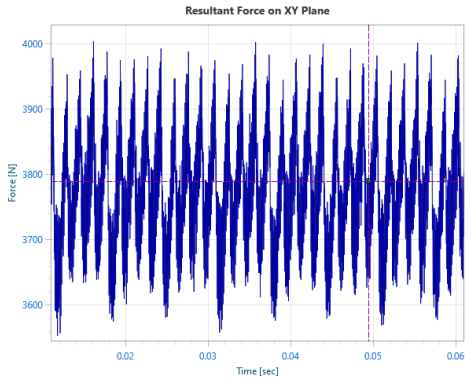

Figure 18 Resultant cutting forces for Tool 1 (CUTPRO).

Similarly, Tool 2 is also simulated as shown in Figure 19, and the chatter free cutting conditions are $n = 11500 rev/\min$, $a_p = 1mm$, $a_e = 15.875mm$. The maximum force is calculated as 183N form CUTPRO, and the maximum bending stress is 22MPa which is very safe.

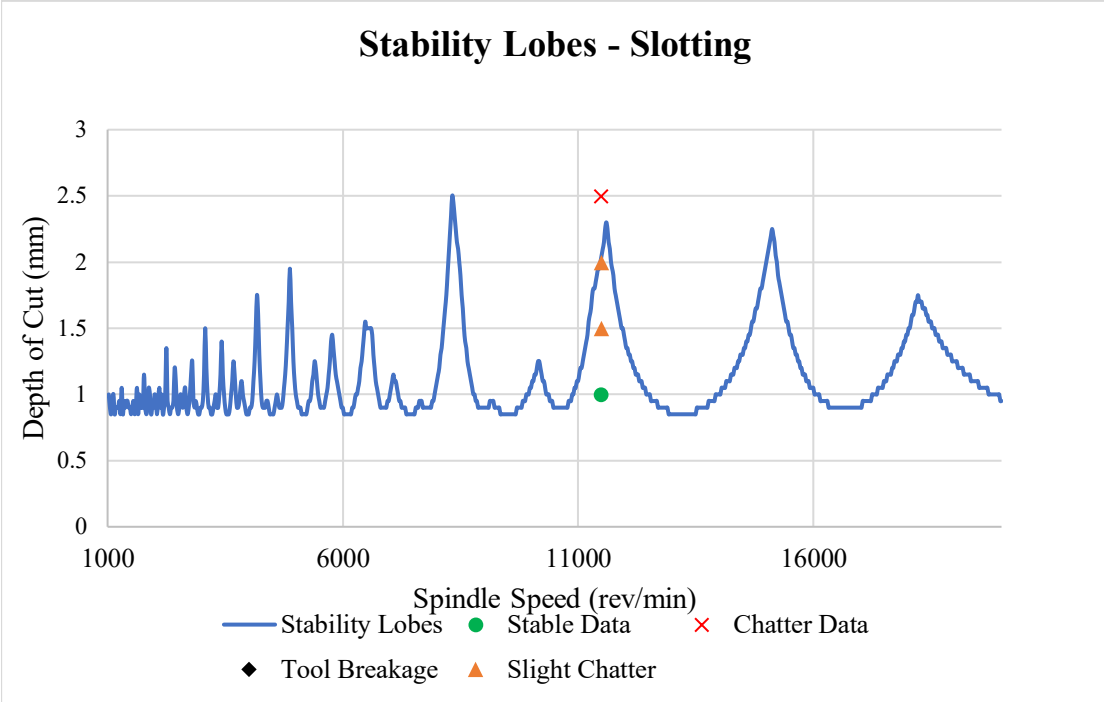

Tool 2 - Stability

Test Number	n [RPM]	a_p [mm]	a_e [mm]	c [/rev/tooth]	Condition
1	11500	2	15.875	0.1	Slight Chatter
2	11500	2.5	15.875	0.1	Chatter
3	11500	1	15.875	0.1	Stable
4	11500	1.5	15.875	0.1	Slight Chatter

Figure 19 Tool 2 stability from CUTPRO. Bullnose end mill with 15.875mm diameter, 2.3mm corner radius and 5 flutes.

Tool 3 is also simulated as shown in Figure 19, and the chatter free cutting conditions are $n = 11800 rev/\min,\ a_p = 12mm,\ a_e = 2mm$. The maximum force is calculated as 600N from CUTPRO, and the maximum bending stress is 275MPa which is safe.

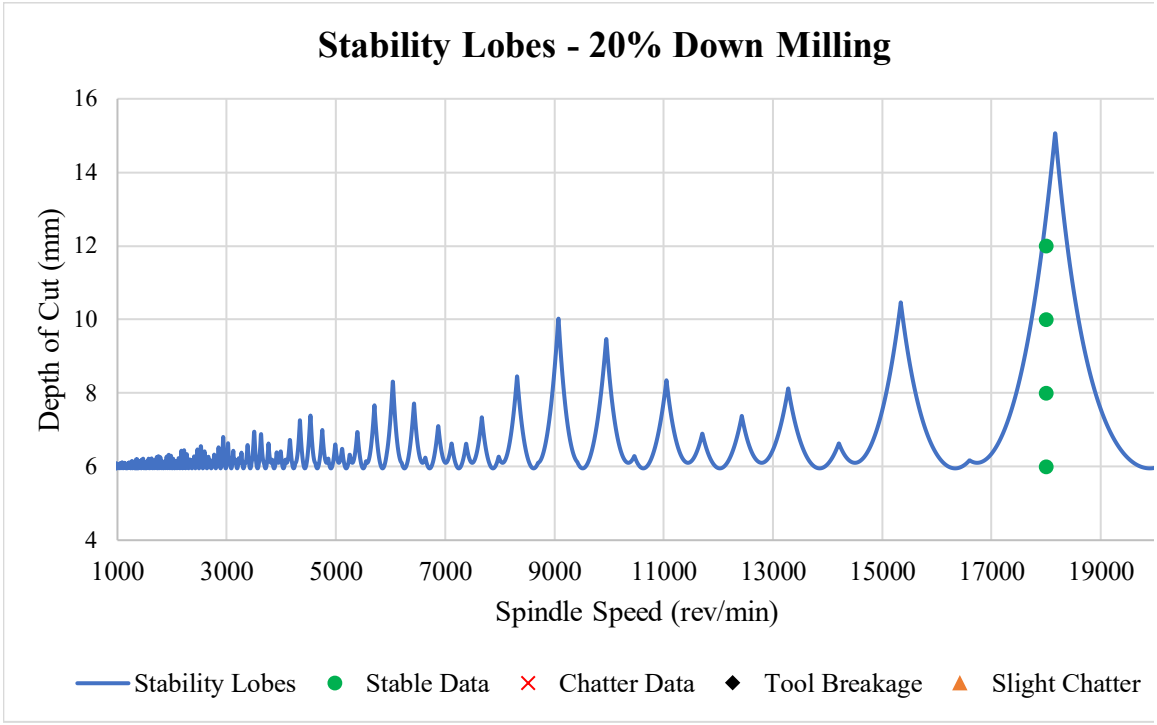

Tool 3 - Stability

Test Number	n [RPM]	a_p [mm]	a_e [mm]	c [mm/rev/tooth]	Condition
1	18000	6	2	0.1	Stable
2	18000	8	2	0.1	Stable
3	18000	10	2	0.1	Stable
4	18000	12	2	0.1	Stable

Figure 20 Tool 3 stability from CUTPRO. End mill with 10mm diameter and 2 flutes.

Tool 4 is also simulated as shown in Figure 19, and the chatter-free cutting conditions are $n = 15300 rev/\min,\ a_p = 1mm,\ a_e = 3mm$. The maximum force is calculated as 126N from CUTPRO, and the maximum bending stress is 55.6MPa which is very safe.

The identified chatter-free and safe cutting conditions are used in NC part programming of the part. Note that these parameters are good only for the machine which is used in FRF testing. If more than one machine has to be used, the process must be repeated for all machines, and cutting conditions that are safe for all machines must be selected.

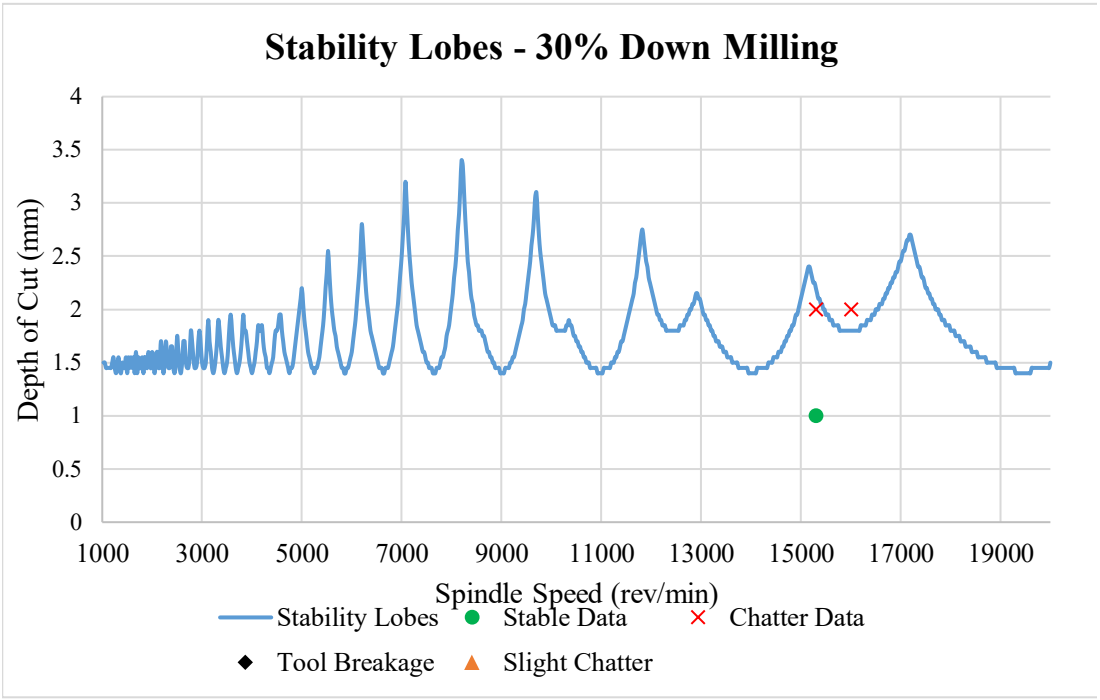

Tool 4 - Stability

Test Number	n [RPM]	a_p [mm]	a_e [mm]	c [mm/rev/tooth]	Condition
1	15300	1	3	0.1	Stable
2	15300	2	3	0.1	Chatter
3	16000	2	3	0.1	Chatter

Figure 21 stability of Tool 4 from CUTPRO. Bullnose end mill with 15.875mm diameter, 2.3mm corner radius and 5 flutes

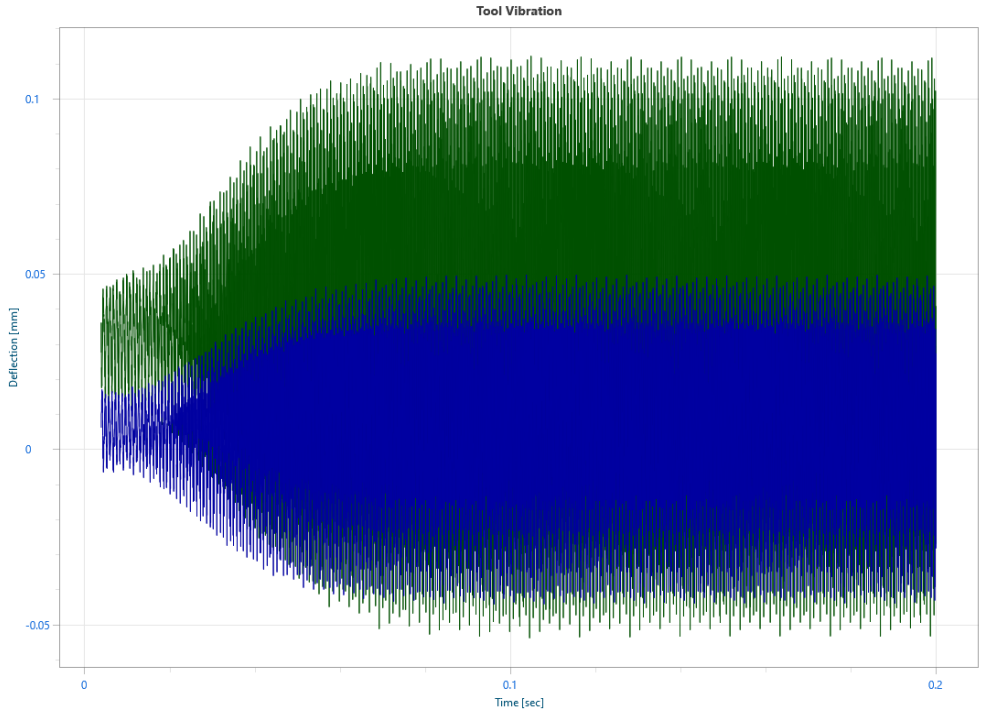
Tool Vibration
0.1
0.05
0
-0.05
Deflection [mm]
0
0.1
0.2
Time [sec]

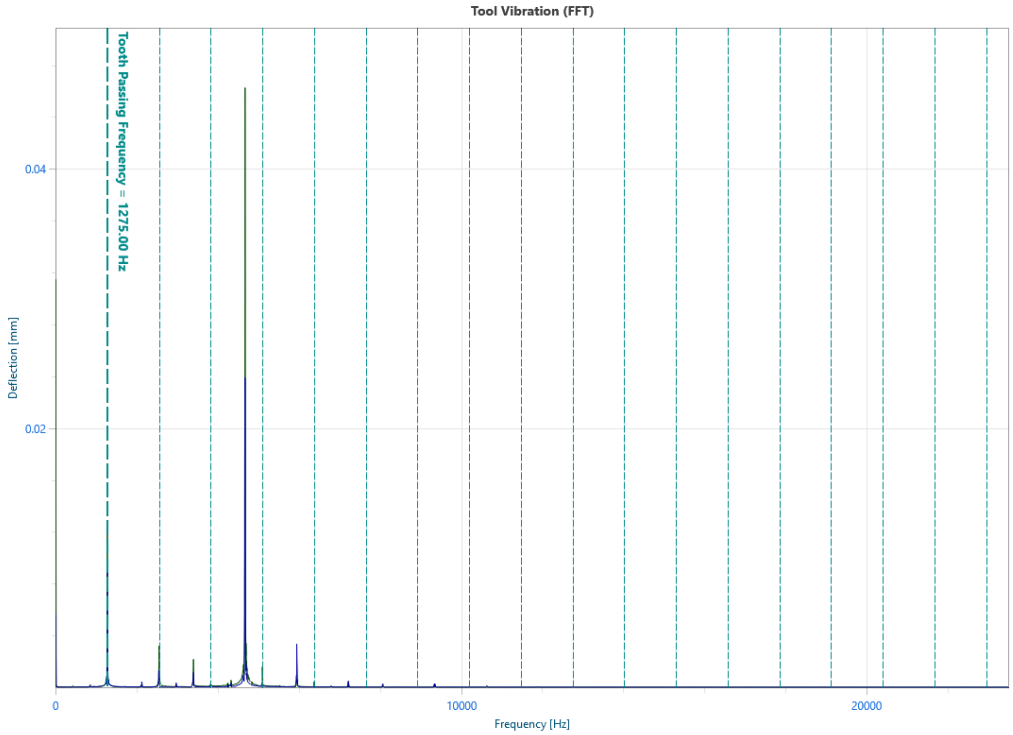
Tool Vibration (FFT)
Tooth Passing Frequency = 1275.00 Hz
0.04
0.02
Deflection [mm]
0
10000
20000
Frequency [Hz]

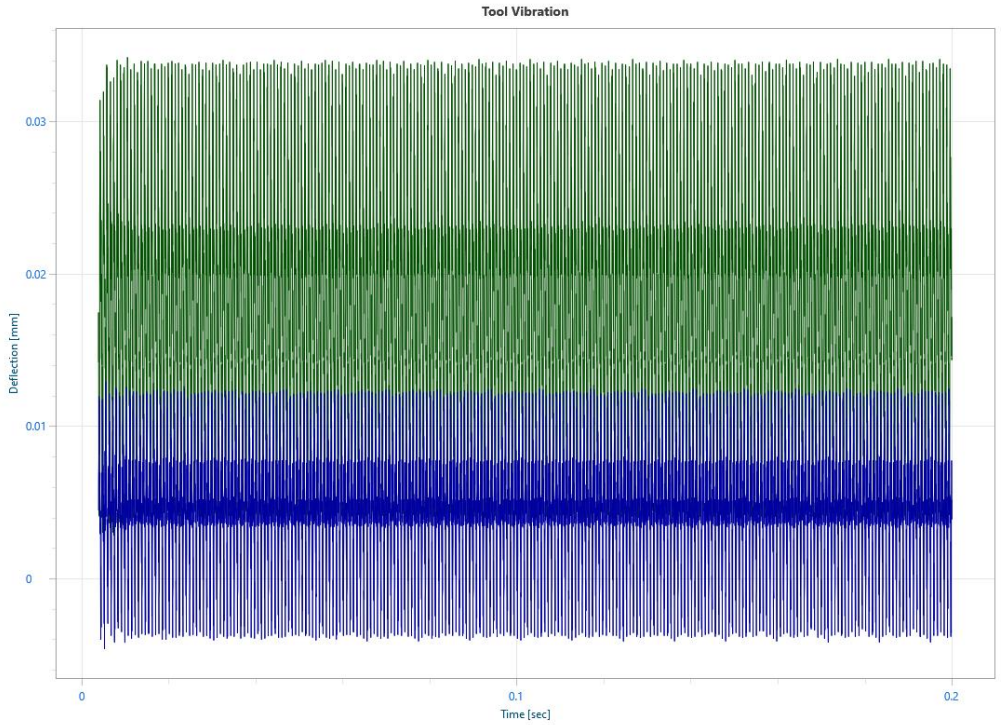

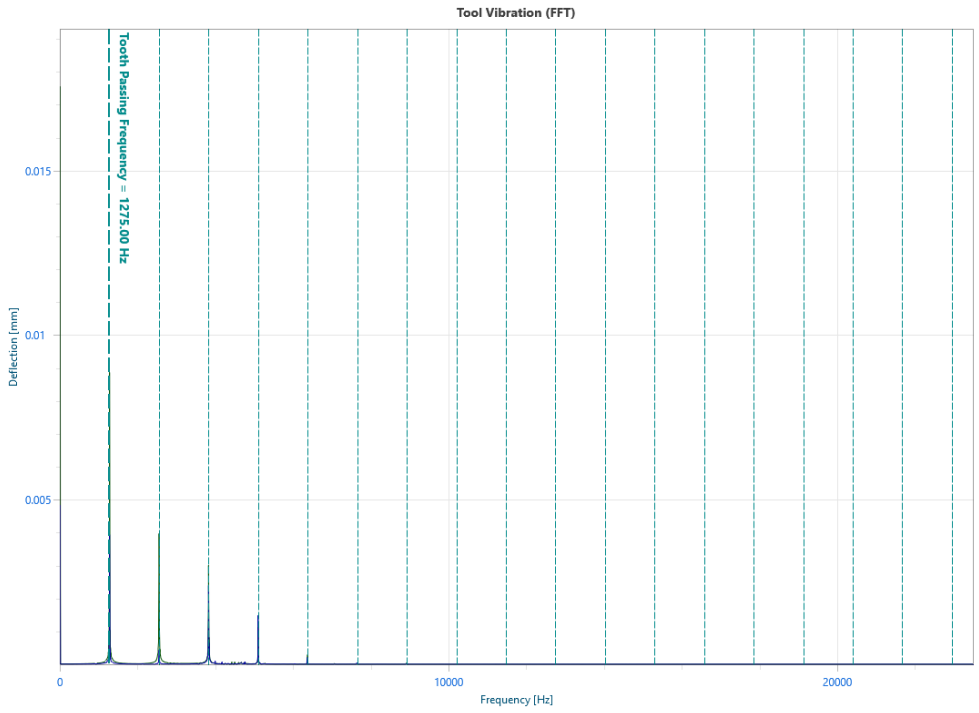

Chapter 4 – Toolpath Generation using NX CAM

The chatter free, optima and safe stable cutting conditions shown in Table 6 are entered into NX CAM software to generate toolpaths. The first tool is serrated and used for heavy duty roughing operation which requires the highest torque and power, but they are within the capacity of the spindle of DMU 50 CNC machining center.

Table 6 Optimal and safe cutting conditions selected from stability lobes and CUTPRO.

Tool Number	n Spindle Speed [rev/min]	a_p depth [mm]	a_e width [mm]	c feedrate [mm/rev /tooth]	Avrg. Torque [N/m]	Avrg. Power [Kw]	Condition
1	9180	36	10	0.1	37.7387	36.2795	Stable
2	11500	1	15.875	0.1	1.6743	1.8955	Stable
3	18000	12	2	0.1	1.2488	2.3530	Stable
4	15300	1	3	0.1	0.3003	0.4807	Stable

The blank workpiece was a rectangular Aluminum 7050 block with dimensions 155mm x 107mm x 45mm. The screenshots of machining operations in NX CAM system are shown in Figure 22, cutting conditions are given in Table 6, and the operations are listed as follows:

Operation 1- Opening a hole in the block: First a hole is opened in the block by the helical–orbital milling cycle. The hole is used for the end mill entry for roughing. A helical end mill with (Tool #2) 5 plunging style cutting edges is used in opening the hole.

Operation 2- Roughing the pockets: The internal pockets are rough milled with the serrated Tool #1 at the spindle speed of 9180 rev/min, 0.1 mm/rev/tooth feedrate, 36 mm axial and 10 mm radial depth of cut as shown in Figure 22. Four fluted serrated tool has a 20 mm diameter as listed in Table 1. About 2 mm of stock was left on the walls, and 0 mm was left at the bottom of the cavities.

Operation 3- Semi-finishing the walls: The walls are semi-finished with Tool 3, and 1.25 mm stock was left on the walls.

Operation 4- Roughing roots: Roots connecting the walls with the floor are roughed with Tool 3 having 10 mm diameter, leaving zero floor stock. However, the tool does not have a bull nose corner to finish the wall-floor roots.

Operation 5- Finishing walls: Walls are finished with 10 mm diameter end mill (Tool 3).

Operation 6- Semi-finishing roots: End mill with 10 mm diameter (Tool 3) is used to semi-finish the leftover stock at the roots. Since the tool is sharp there needs to be one more pass with another tool to finish the roots.

Operation 7- Finishing roots: – Finishing the roots with bull nose end mill (Tool 4) in one pass which has the same corner radius of 2.3mm as the roots are making with the floor.

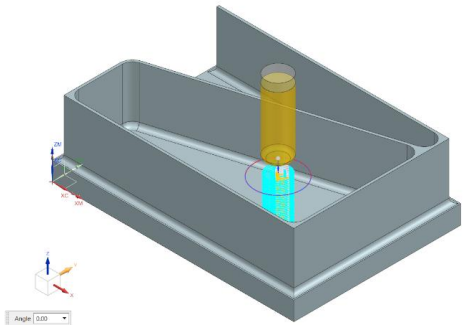

Operation 1: Orbital drilling of hole (Tool 2)

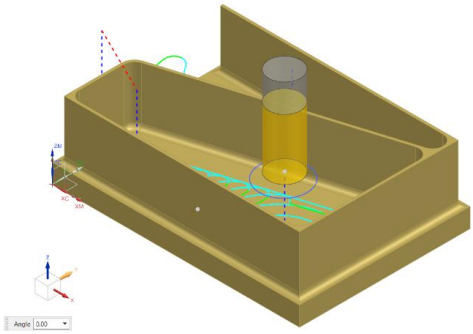

Operation 2: Pocketing cavities with serrated Tool 1

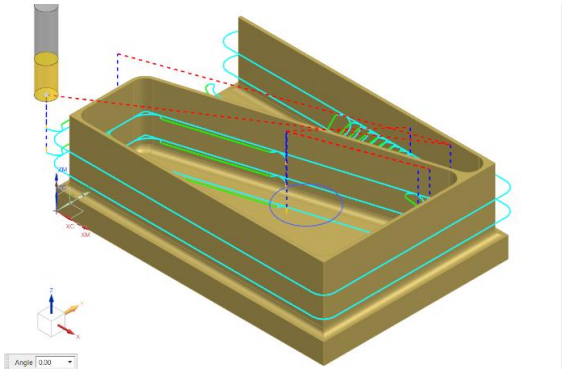

Operation 3: Semi-roughing walls and floors with Tool 3.

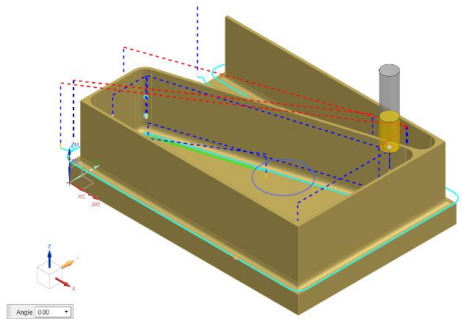

Operation 4: Roughing roots of the walls with Tool 3.

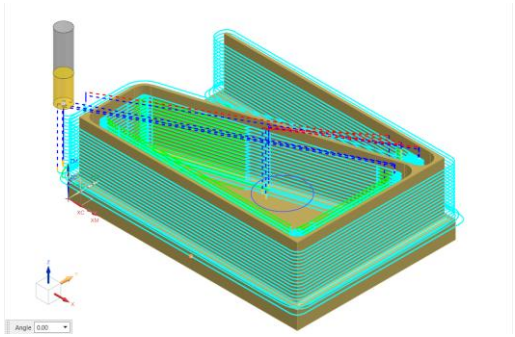

Operation 5: Finishing walls with Tool 3.

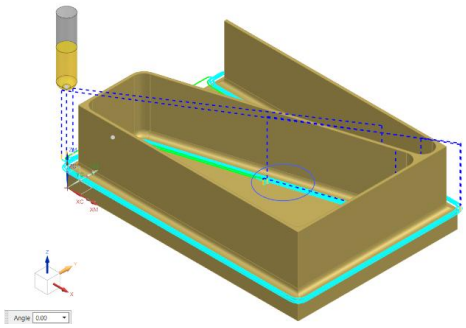

Operation 6: Semi- finishing roots with Tool 3.

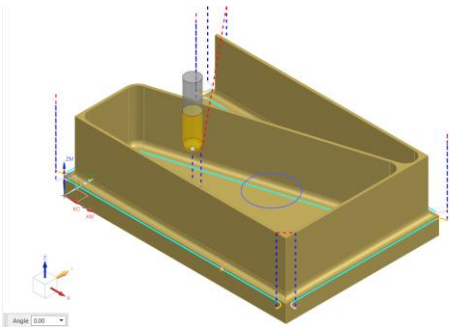

Operation 7: Finishing roots with Tool 4.

Figure 22 Machining operations for the thin walled part.

Chapter 5 – Toolpath Optimization using Npro NX Plugin

MAL Inc integrated its physics-based part machining process simulation and optimization algorithms into NX CAM system which is called as ***NPRO***. NPRO displays the chip loads, forces, torque, and power along the tool path. The user can set maximum chip thickness, force, torque, and power and NPRO automatically schedules the feed along the tool path to further optimize the machining cycle time. Similar to CUTPRO, NPRO accepts the work material's cutting force coefficients, and tool's helix and rake angles, and the number of flutes. The user can also enter the spindle's speed-dependent torque and power limits, the acceleration and jerk limits set in the CNC. It has a built-in virtual CNC which improves the estimation of real feed and machining cycle times. NPRO breaks up long tool paths into shorter ones and varies the feed for each path segment.

In this 3-axis machining of the thin-walled part, the cutter–part engagement geometry along the tool path does not vary much, therefore there will be hardly any optimization opportunity here. NPRO can improve productivity up to 40-60%, especially in 5-axis machining of dies, molds, and gas turbine parts with sharp curvatures which causes frequent changes in the chip thickness along the tool paths. Here, only the roughing operation is attempted to be optimized by setting chip thickness, and the spindle's torque and power limits as shown in Figure 24. Only the roughing (Operations 2 and 4), and semi- roughing (operations 3,6) are optimized here. Finishing is not optimized to avoid leaving feed marks on the surface finish. NPro reduced the machining times as shown in NX screen shot (Figure 25) and listed as follows:

Operation 2: Cycle time is reduced from 28 seconds to 26 seconds (+9.55% productivity gain).

Operation 3: Cycle time is reduced from 1':16" to 47 seconds (+59.20% productivity gain)

Operation 4: Cycle time is reduced from 32 seconds to 21 seconds (+49.52 % productivity gain)

Operation 6: Cycle time is reduced from 1':12" to 35 seconds (+105.73 % productivity gain)

Chatter stability, spindle torque and power, and chip load limits are also satisfied with the optimized NC part program using NPRO.

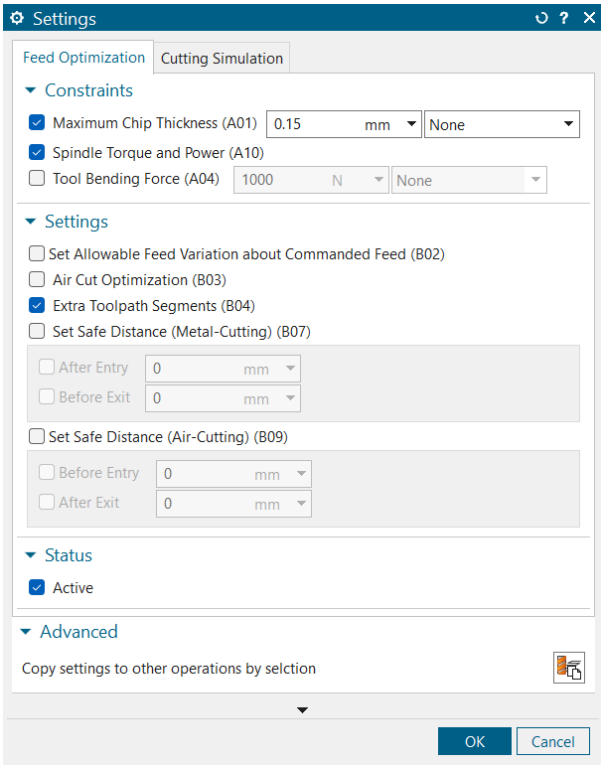

Figure 24 NPRO settings: Chip thickness is set to 0.15mm, and spindle's torque and power limits are used in optimization.

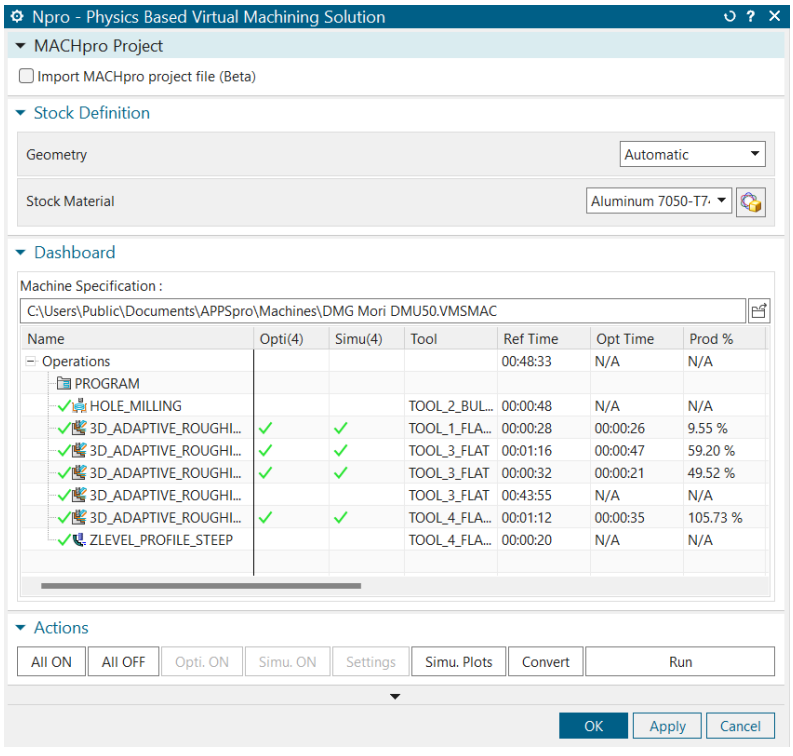

Figure 25 NX – NPRO screen shot, showing all operations with original and optimized cycle times.

Chapter 6 – Part Machining

The optimized tool path within NX NPRO is postprocessed to be machined on DMG Mori DMU 50 Five-axis CNC machining center at UBC Manufacturing Automation Laboratory. The machine was operated by the research engineer Nima Dabiri as the authorized user. Since only the upper side of the stock is machined, the blank is mounted on a wise as shown in Figure 26. The postprocessed NC part program or G code is given in Appendix B.

First, air-cutting test was conducted to ensure the setup and NC part program is collision-free. The part program was collision-free, and the part was machined in 32 minutes and 40

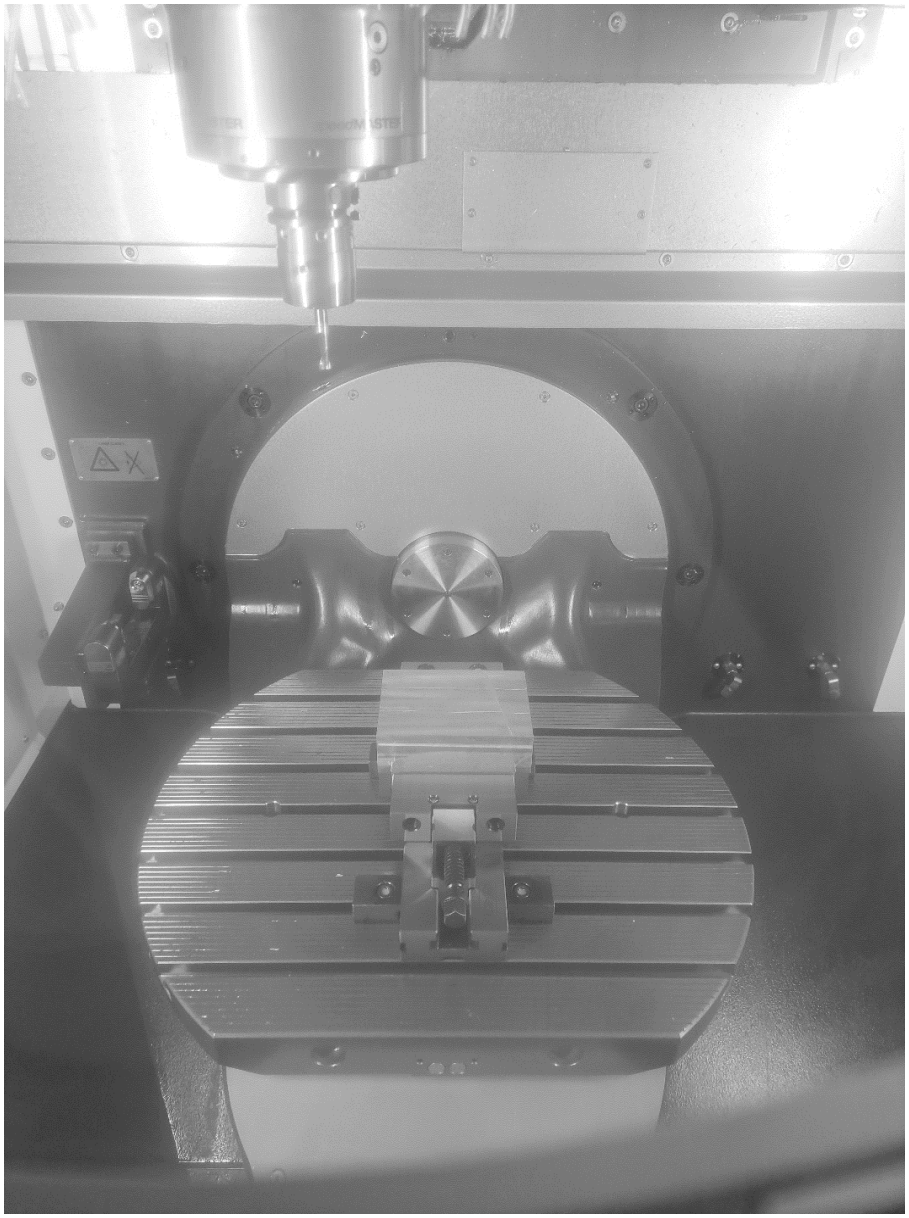

Figure 26 Stock material setup in a vice on DMU 50 Five Axis CNC Machining center.

seconds. The part is air cut without NPRO optimization as well, and it took 33 minutes 21 seconds. It is natural that the actual machining times are never equal to CAM predicted cycle times, because CAM systems neglect the acceleration and deceleration profiles of the real machine. Since the major optimization is done using CUTPRO, and the tool paths were mostly linear (G01) paths, the optimized cycle time difference is small. If the part had many 5 axis motions, the gain cycle time would be higher.

The part is successfully machined at the first trial without any chatter, tool breakage and violation of spindle limits, see Figure 27. In short, the most optimal NC part program is generated and the part is machined correctly and optimally in the first trial without iterating in trial and error tests.

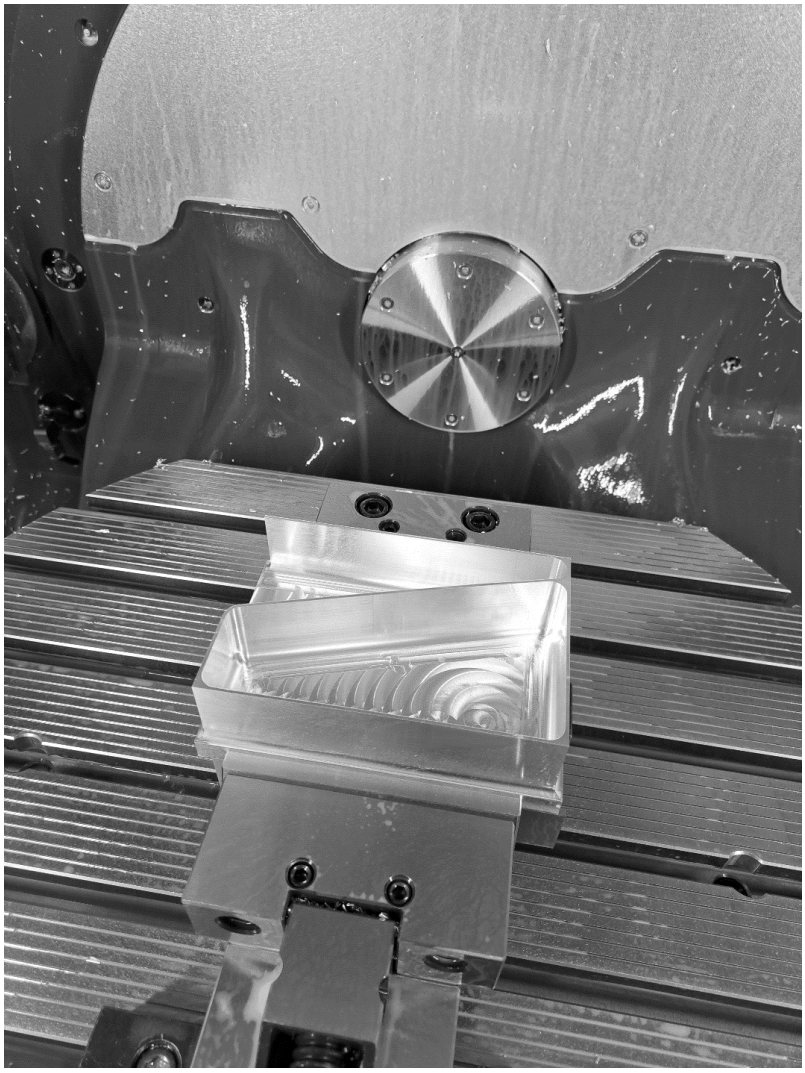

Figure 27 Finished thin walled workpiece.

Chapter 7- Conclusion

This project shows how part machining can be planned using physics-based, advanced engineering techniques developed at the University of British Columbia. The machine is tap-tested to find its natural frequencies and stiffness with each tool, followed by the prediction of chatter-free cutting conditions. The part program is generated by selecting these optimal cutting conditions that do not lead to chatter and tool breakage while not exceeding the spindle's torque and power limits. The part is virtually cut in CAM environment to observe forces, torque, and power. It is also automatically optimized by varying the feed along the tool path while keeping the chip load at the desired levels but without violating the spindle's torque and power limits. As a result, the part is machined without any problem and most optimally at the first trial, hence avoiding experience-based trial and error approaches used in industry.

In conclusion, using advanced digital machining methods proved to be valuable for cost savings during machining. Depending on the part, the machining cycle times can be reduced, and the scrap rate is eliminated or reduced significantly, leading to cost reduction.

References

[1] Altintas, Y. (n.d.). Manufacturing Automation (second). Cambridge University Press.
[2] Y. Altintas, Advanced Machining Course Notes for industry, 2023, MAL Inc.
[3] CUTPRO(TM) Advanced Machining Simulation System, MAL Inc. www.malinc.com
[4] NPRO NX Integrated Process Simulation and Optimization Software, www.malinc.com

Appendix A – Stability code in MATLAB

```
%BCIT final project-chatter stability program
%Hasan Altan Altintas A00711066
%Jan 3rd 2024
% This program uses approximate singel point stability of
Tlusty
clear all;
close all;
pi=3.14159265;
s=tf('s') ;
% structural modes
% mode #1 wn1(Hz) k(N/m)
wn(1)=2836*2*pi    ; zeta(1)=0.0177 ; k(1)=70.44E06 ;
wn(2)=4137*2*pi    ; zeta(2)=0.0254 ; k(2)=76.81E06 ;
wn(3)=4865*2*pi    ; zeta(3)=0.0153 ; k(3)=98.64E06 ;
% transfer functions
wc1=2500;wc2=5200;  %Hz

for ii=1:6000
    wc=ii*2*pi;  % Frequency in rad/s
    w(ii)=ii; %Frequency in Hz
    GR=0; HI=0 ; %Initialize the real and imaginary parts to
zero for the frequency wc;
  for  n=1:3
    DEN=k(n)*((wn(n)^2-wc^2)^2+(2*zeta(n)*wn(n)*wc)^2);
    GR=GR+wn(n)^2*(wn(n)^2-wc^2)/DEN;
    HI=HI-(wn(n)^2)*(2*zeta(n)*wn(n)*wc)/DEN;
  end
  G(ii)=GR;
  H(ii)=HI;
end
figure (1);
subplot(2,1,1);
       plot(w,G);
     title('Real Part of the FRF');
     xlabel('Frequency [Hz]');
          ylabel('G(w) [m/N]');
  subplot(2,1,2);
       plot(w,H);
           title('Imaginary Part of the FRF');
     xlabel('Frequency [Hz]');
     ylabel('H(w) [m/N]')

    %stability
   % Cutting coefficeints
   Ktc=850e6; Krc=200e6;
   N=5 ; % Number of teeth
   D=15.875 ; % mm tool diameter
   b=15.875 ; % width of cut
   me=(b/D)*(N/2);  % scaling ratioop for width of cut
m=0;
for ii=1:6000
    wc=ii*2*pi;  % Frequency in rad/s
    if G(ii)<0
```

```
    m=m+1
  for  kk=1:10
   alim(m,kk)=-1/(2*Ktc*G(ii)*me);
   psi=atan2(H(ii),G(ii)); % Phase
   eps=2*psi+pi;
   T=(2*pi*kk+eps)/wc; % Tooth period
   n(m,kk)=60/(N*T) ;    % spindle speed
  end
    end
end
figure (2);
plot(n,alim, 'b.');
xlim([4000 20000]);
ylim([0,0.005]);
      title('Stability');
     xlabel('Spindle Speed [rev/min]');
     ylabel('Depth of cut [m]')
```

Appendix B – NC part program sample (CL File) in NX NPRO.

TOOL PATH/3D_ADAPTIVE_ROUGHING_FLATSEMIFINISH,TOOL,TOOL_3_FLAT

TLDATA/MILL,9.9740000,0.0000000,44.9000000,0.0000000,0.0000000

MSYS/0.0000000,0.0000000,0.0000000,1.0000000,0.0000000,0.0000000,0.0000000,1
.0000000,0.0000000

$$ centerline data

PAINT/PATH

PAINT/SPEED,10

LOAD/TOOL,3

SELECT/TOOL,3

SPINDL/RPM,18000,CLW

PAINT/COLOR,186

RAPID

GOTO/-4.8229892,2.1091690,53.0000004,0.0000000,0.0000000,1.0000000

PAINT/COLOR,211

RAPID

GOTO/-4.8229892,2.1091690,49.0000004

PAINT/COLOR,42

FEDRAT/MMPM,1800.00000

GOTO/-4.8229892,2.1091690,46.0000004

PAINT/COLOR,31

GOTO/-3.4818333,1.9659791,46.0000004

CIRCLE/-3.3749050,2.9676839,46.0000004,0.0000000,0.0000000,-
1.0000000,1.0073957,0.0200000,0.5000000,9.9740000,0.0000000

GOTO/-2.3888573,2.7613927,46.0000004

CIRCLE/-20.627411,6.1422918,46.0000004,0.0000000,0.0000000,-
1.0000000,18.5492676,0.0200000,0.5000000,9.9740000,0.0000000

GOTO/-2.0869126,5.5719930,46.0000004

CIRCLE/-147.66126,10.7942121,46.0000004,0.0000000,0.0000000,-1.0000000,145.667988,0.0200000,0.5000000,9.9740000,0.0000000

GOTO/-1.9937456,11.1649234,46.0000004

GOTO/-1.9876428,15.0796149,46.0000004

GOTO/-1.9842537,37.8328009,46.0000004

CIRCLE/20.2648091,38.0125320,46.0000004,0.0000000,0.0000000,1.0000000,22.2497887,0.0200000,0.5000000,9.9740000,0.0000000

GOTO/-1.7105650,41.4962127,46.0000004

CIRCLE/12.0409589,39.4030237,46.0000004,0.0000000,0.0000000,1.0000000,13.9099192,0.0200000,0.5000000,9.9740000,0.0000000

GOTO/6.0364277,51.9501930,46.0000004

CIRCLE/19.6311460,23.3739086,46.0000004,0.0000000,0.0000000,1.0000000,31.6452270,0.0200000,0.5000000,9.9740000,0.0000000

GOTO/9.8053663,53.4550397,46.0000004

CIRCLE/101.954216,-225.43990,46.0000004,0.0000000,0.0000000,1.0000000,293.724017,0.0200000,0.5000000,9.9740000,0.0000000

GOTO/17.1831795,55.7853998,46.0000004

GOTO/135.639491,92.1181510,46.0000004

CIRCLE/134.016224,97.5871432,46.0000004,0.0000000,0.0000000,-1.0000000,5.7048110,0.0200000,0.5000000,9.9740000,0.0000000

GOTO/137.283698,92.9107680,46.0000004

CIRCLE/136.256456,94.3603182,46.0000004,0.0000000,0.0000000,-1.0000000,1.7766320,0.0200000,0.5000000,9.9740000,0.0000000

GOTO/137.990590,93.9740542,46.0000004

CIRCLE/136.647423,94.2352978,46.0000004,0.0000000,0.0000000,-1.0000000,1.3683375,0.0200000,0.5000000,9.9740000,0.0000000

GOTO/137.926483,94.7214594,46.0000004

CIRCLE/136.045047,93.7398133,46.0000004,0.0000000,0.0000000,-1.0000000,2.1221284,0.0200000,0.5000000,9.9740000,0.0000000

GOTO/137.433949,95.3443010,46.0000004

CIRCLE/136.328107,93.5346806,46.0000004,0.0000000,0.0000000,-1.0000000,2.1207575,0.0200000,0.5000000,9.9740000,0.0000000

GOTO/136.743967,95.6142653,46.0000004

CIRCLE/134.061185,82.6495287,46.0000004,0.0000000,0.0000000,-1.0000000,13.2394002,0.0200000,0.5000000,9.9740000,0.0000000

GOTO/134.718510,95.8726011,46.0000004

CIRCLE/130.321524,17.1422017,46.0000004,0.0000000,0.0000000,-1.0000000,78.8530866,0.0200000,0.5000000,9.9740000,0.0000000

GOTO/130.446105,95.9951899,46.0000004

CIRCLE/124.394261,-774.84311,46.0000004,0.0000000,0.0000000,-1.0000000,870.859335,0.0200000,0.5000000,9.9740000,0.0000000

GOTO/121.767564,96.0122568,46.0000004

GOTO/73.3814481,96.0134126,46.0000004

GOTO/5.6307548,96.0216540,46.0000004

CIRCLE/5.5974379,103.858413,46.0000004,0.0000000,0.0000000,1.0000000,7.8368305,0.0200000,0.5000000,9.9740000,0.0000000

GOTO/3.1774048,96.4045990,46.0000004

CIRCLE/5.1023194,102.034247,46.0000004,0.0000000,0.0000000,1.0000000,5.9496419,0.0200000,0.5000000,9.9740000,0.0000000

GOTO/1.4914310,97.3056406,46.0000004

CIRCLE/3.7894936,101.788192,46.0000004,0.0000000,0.0000000,1.0000000,5.0372968,0.0200000,0.5000000,9.9740000,0.0000000

GOTO/-1.0608527,100.428596,46.0000004

CIRCLE/4.7218614,102.178492,46.0000004,0.0000000,0.0000000,1.0000000,6.0416816,0.0200000,0.5000000,9.9740000,0.0000000

GOTO/-1.2353433,103.185283,46.0000004

CIRCLE/3.7700668,103.238418,46.0000004,0.0000000,0.0000000,1.0000000,5.0056922,0.0200000,0.5000000,9.9740000,0.0000000

GOTO/2.1074069,107.959913,46.0000004

CIRCLE/6.8760815,94.4004739,46.0000004,0.0000000,0.0000000,1.0000000,14.3735404,0.0200000,0.5000000,9.9740000,0.0000000

GOTO/5.3841294,108.696373,46.0000004

CIRCLE/9.5460146,71.9959386,46.0000004,0.0000000,0.0000000,1.0000000,36.9356630,0.0200000,0.5000000,9.9740000,0.0000000

GOTO/8.9908554,108.927429,46.0000004

CIRCLE/14.7894725,-191.59630,46.0000004,0.0000000,0.0000000,1.0000000,300.579666,0.0200000,0.500000,9.9740000,0.0000000

GOTO/15.7229242,108.981916,46.0000004

GOTO/149.291485,108.983358,46.0000004

CIRCLE/149.346043,100.644376,46.0000004,0.0000000,0.0000000,1.0000000,8.3391598,0.0200000,0.5000000,9.9740000,0.0000000

GOTO/151.570758,108.681306,46.0000004

CIRCLE/149.837734,102.831156,46.0000004,0.0000000,0.0000000,1.0000000,6.1014446,0.0200000,0.5000000,9.9740000,0.0000000

GOTO/153.558434,107.666858,46.0000004

CIRCLE/151.232682,103.227897,46.0000004,0.0000000,0.0000000,1.0000000,5.0113368,0.0200000,0.5000000,9.9740000,0.0000000

GOTO/155.969090,104.864948,46.0000004

CIRCLE/142.305605,100.102833,46.0000004,0.0000000,0.0000000,1.0000000,14.4695738,0.0200000,0.5000000,9.9740000,0.0000000

GOTO/156.698899,101.586627,46.0000004

CIRCLE/119.199156,97.3922853,46.0000004,0.0000000,0.0000000,1.0000000,37.7335821,0.0200000,0.5000000,9.9740000,0.0000000

GOTO/156.929084,97.9174009,46.0000004

Appendix C– Post processed NC part program sample

```
; PROGRAM NUMBER: Part_NPRO.MPF
; PART      NAME:       Part_CAM.prt
; PROGRAM   UNIT: MM
; PROGRAMMED  BY: NIMADF
; PROGRAMMED  ON: MON OCT 23,2023, 16:54
; MACHINE   NAME: DMU-50-5AXIS-MILL-MM, SIEMENS-840D
; NX  POST  NAME: DMU50_5AXIS_SIEMENS840D_MM_NEW, REV: JULY-21ST-2023
;
; ----------TOOL LIST----------
; 5_8INCH_BULLNOSE_ENDMILL  | DIA=15.8300 | CR=2.3000
; 20MM_SERRATED_FLAT_ENDMILL | DIA=20.0000 | CR=0.0000
; 10MM_FLAT_ENDMILL         | DIA=9.9740 | CR=0.0000
; 10MM_RADIUS_ENDMILL       | DIA=10.0100 | CR=3.0000
;


;
;Start of Program
;

N1 G90 G40 G17 G710 G94
N2 CYCLE800()
N3 CYCLE832(0.,_OFF,1)
N4 TRAFOOF
N5 TRANS
;
N6 G54
;
```

```
; @-OPER: HOLE_MILLING
;
N7 T="5_8INCH_BULLNOSE_ENDMILL"
N8 M6
N9 D1
; TOOL NAME: 5_8INCH_BULLNOSE_ENDMILL
; TOOL-DESC: MILLING TOOL-5 PARAMETERS
; TOOL- DIA: 15.830
; LENGTH OF CUT: 50.000
; CORNER  RADII: 2.300

N10 ;TOOL,TOOL_2_BULLNOSE
N11 ;TLDATA/MILL,15.8750,2.3000,47.1000,0.0000,0.0000
N12 ;$$ centerline data
N10 G90 G54
N11 S11500 M3 M8
N12 G0 B0.0 C0.0
N13 TRAFOOF
N14 M22
N15 G0 X117.344 Y27.4976
N16 Z51.
N17 G3 X120.8752 Y27.4976 I1.7656 J0.0 F5750.
N18 X117.3003 Y31.0285 Z50. I-3.5312 J0.0 TURN=0
N19 X117.3003 Y31.0285 I.0437 J-3.531
N20 X117.344 Y27.4976 I.0218 J-1.7655
N21 G0 Z51.
N22 G3 X124.4065 Y27.4976 I3.5312 J0.0
N23 X117.2566 Y34.5595 Z50. I-7.0625 J0.0 TURN=0
N24 X117.2566 Y34.5595 I.0874 J-7.062
```

N25 X117.344 Y27.4976 I.0437 J-3.531

N26 X120.8752 Y27.4976 I1.7656 J0.0

N27 X117.3003 Y31.0285 Z49. I-3.5312 J0.0 TURN=0

N28 X117.3003 Y31.0285 I.0437 J-3.531

N29 X117.344 Y27.4976 I.0218 J-1.7655

N30 G0 Z50.

N31 G3 X124.4065 Y27.4976 I3.5312 J0.0

N32 X117.2566 Y34.5595 Z49. I-7.0625 J0.0 TURN=0

N33 X117.2566 Y34.5595 I.0874 J-7.062

N34 X117.344 Y27.4976 I.0437 J-3.531

N35 X120.8752 Y27.4976 I1.7656 J0.0

N36 X117.3003 Y31.0285 Z48. I-3.5312 J0.0 TURN=0

N37 X117.3003 Y31.0285 I.0437 J-3.531

N38 X117.344 Y27.4976 I.0218 J-1.7655

N39 G0 Z49.

N40 G3 X124.4065 Y27.4976 I3.5312 J0.0

N41 X117.2566 Y34.5595 Z48. I-7.0625 J0.0 TURN=0

N42 X117.2566 Y34.5595 I.0874 J-7.062

N43 X117.344 Y27.4976 I.0437 J-3.531

N44 X120.8752 Y27.4976 I1.7656 J0.0

N45 X117.3003 Y31.0285 Z47. I-3.5312 J0.0 TURN=0

N46 X117.3003 Y31.0285 I.0437 J-3.531

N47 X117.344 Y27.4976 I.0218 J-1.7655

N48 G0 Z48.

N49 G3 X124.4065 Y27.4976 I3.5312 J0.0

N50 X117.2566 Y34.5595 Z47. I-7.0625 J0.0 TURN=0

N51 X117.2566 Y34.5595 I.0874 J-7.062

N52 X117.344 Y27.4976 I.0437 J-3.531

N53 X120.8752 Y27.4976 I1.7656 J0.0

N54 X117.3003 Y31.0285 Z46. I-3.5312 J0.0 TURN=0

N55 X117.3003 Y31.0285 I.0437 J-3.531

N56 X117.344 Y27.4976 I.0218 J-1.7655

N57 G0 Z47.

N58 G3 X124.4065 Y27.4976 I3.5312 J0.0

N59 X117.2566 Y34.5595 Z46. I-7.0625 J0.0 TURN=0

N60 X117.2566 Y34.5595 I.0874 J-7.062

N61 X117.344 Y27.4976 I.0437 J-3.531

N62 X120.8752 Y27.4976 I1.7656 J0.0

N63 X117.3003 Y31.0285 Z45. I-3.5312 J0.0 TURN=0

N64 X117.3003 Y31.0285 I.0437 J-3.531

N65 X117.344 Y27.4976 I.0218 J-1.7655

N66 G0 Z46.

N67 G3 X124.4065 Y27.4976 I3.5312 J0.0

N68 X117.2566 Y34.5595 Z45. I-7.0625 J0.0 TURN=0

N69 X117.2566 Y34.5595 I.0874 J-7.062

N70 X117.344 Y27.4976 I.0437 J-3.531

N71 X120.8752 Y27.4976 I1.7656 J0.0

N72 X117.3003 Y31.0285 Z44. I-3.5312 J0.0 TURN=0

N73 X117.3003 Y31.0285 I.0437 J-3.531

N74 X117.344 Y27.4976 I.0218 J-1.7655

N75 G0 Z45.

N76 G3 X124.4065 Y27.4976 I3.5312 J0.0

N77 X117.2566 Y34.5595 Z44. I-7.0625 J0.0 TURN=0

N78 X117.2566 Y34.5595 I.0874 J-7.062

N79 X117.344 Y27.4976 I.0437 J-3.531

N80 X120.8752 Y27.4976 I1.7656 J0.0

N81 X117.3003 Y31.0285 Z43. I-3.5312 J0.0 TURN=0

N82 X117.3003 Y31.0285 I.0437 J-3.531

N83 X117.344 Y27.4976 I.0218 J-1.7655

N84 G0 Z44.

N85 G3 X124.4065 Y27.4976 I3.5312 J0.0

N86 X117.2566 Y34.5595 Z43. I-7.0625 J0.0 TURN=0

N87 X117.2566 Y34.5595 I.0874 J-7.062

N88 X117.344 Y27.4976 I.0437 J-3.531

N89 X120.8752 Y27.4976 I1.7656 J0.0

N90 X117.3003 Y31.0285 Z42. I-3.5312 J0.0 TURN=0

N91 X117.3003 Y31.0285 I.0437 J-3.531

N92 X117.344 Y27.4976 I.0218 J-1.7655

N93 G0 Z43.

N94 G3 X124.4065 Y27.4976 I3.5312 J0.0

N95 X117.2566 Y34.5595 Z42. I-7.0625 J0.0 TURN=0